Magnetic Reconnection in Astrophysical and Laboratory Plasmas

Ellen G. Zweibel[1] and Masaaki Yamada[2]

[1]Departments of Astronomy & Physics, University of Wisconsin-Madison, Wisconsin 53706; email: zweibel@astro.wisc.edu

[2]Princeton Plasma Physics Laboratory, Princeton University, Princeton, New Jersey; email: myamada@pppl.gov

Annu. Rev. Astron. Astrophys. 2009. 47:291–332

The *Annual Review of Astronomy and Astrophysics* is online at astro.annualreviews.org

This article's doi:
10.1146/annurev-astro-082708-101726

0066-4146/09/0922-0291$20.00

Key Words

laboratory astrophysics, magnetic fields, magnetic reconnection

Abstract

Magnetic reconnection is a topological rearrangement of magnetic field that converts magnetic energy to plasma energy. Astrophysical flares, from the Earth's magnetosphere to γ-ray bursts and sawtooth crashes in laboratory plasmas, may all be powered by reconnection. Reconnection is essential for dynamos and the large-scale restructuring known as magnetic self-organization. We review reconnection theory and evidence for it. We emphasize recent developments in two-fluid physics, and the experiments, observations, and simulations that verify two-fluid effects. We discuss novel environments such as line-tied, relativistic, and partially ionized plasmas, focusing on mechanisms that make reconnection fast, as observed. Because there is evidence that fast reconnection in astrophysics requires small-scale structure, we briefly introduce how such structure might develop. Several areas merit attention for astrophysical applications: development of a kinetic model of reconnection to enable spectroscopic predictions, better understanding of the interplay between local and global scales, the role of collisionless reconnection in large systems, and the effects of flows, including turbulence.

1. INTRODUCTION

Magnetic activity underlies many transient phenomena in nature. Solar and stellar flares, magnetospheric substorms, and γ-ray bursts are prominent examples. The magnetic energy that powers these processes is probably released by magnetic reconnection. Because reconnection of magnetic fieldlines alters magnetic topology as well as converts magnetic energy to plasma energy, the generation and evolution of magnetic fields in stars, accretion disks, and galaxies requires magnetic reconnection. Reconnection also occurs in laboratory plasmas. It plays a key role in the self-organization of fusion plasmas where plasma current is used to form and confine the plasma. Sawtooth oscillations, in which the plasma current profile periodically self-organizes through reconnection, is a typical example. Strong interest in the fundamental physics of reconnection has recently triggered a series of dedicated experiments to study reconnection under controlled conditions in the laboratory.

Traditionally, reconnection has been described in the magnetohydrodynamic (MHD) regime. To an excellent approximation, magnetic fieldlines are frozen to the plasma and magnetic flux is conserved. In this context, reconnection refers to the breakdown of the frozen magnetic flux condition on timescales much shorter than the plasma's classical diffusion time based on electron-ion collisions. Magnetic fieldlines are frozen to the plasma everywhere but in a small diffusion region, in which the lines break. In the collisionless, non-MHD regime, this description must be modified to accommodate recent developments in two-fluid physics and microscopic anisotropies introduced by the magnetic field direction. But if we stipulate that "frozen" means frozen to the electrons, and recognize that electron inertia and stress can also remove the frozen field constraint, our definition remains valid. In particular, the definition implies that reconnection requires multiple spatial scales: a tiny region within which the frozen field condition is violated, as well as a global region that feeds magnetic fieldlines to the small scales where they break and reconnect. This makes reconnection challenging to observe directly, and to calculate numerically. It also requires us to address the origin of this small-scale structure.

In addition to the length scale problem, there is a timescale problem. When there is a large disparity between the global and resistive scales, the traditional theory predicts that reconnection is very slow, much slower than the timescales associated with astrophysical transients. How reconnection can be made fast has been the guiding theme of much reconnection research, especially as applied to astrophysics, and is the main focus of this review.

In Section 2, we introduce several theories of reconnection. This provides an interpretive framework for the astronomical observations reviewed in Section 3, as well as the laboratory studies of reconnection described in Section 4. In Section 5 we go more deeply into the theory. Section 6 discusses the interaction between local and global phenomena in reconnection. Section 7 summarizes the status of the subject and the need for future work.

The reconnection literature is vast, and we have not attempted to cover all of it. An earlier *ARAA* review (Bhattacharjee 2004) emphasizes impulsive reconnection in the collisionless regime. A more detailed discussion of reconnection and its global implications, emphasizing laboratory results, is given in Yamada et al. (2009). Pedagogical treatments of reconnection can be found in Biskamp (1993), Priest & Forbes (2000) and Kulsrud (2005).

2. RECONNECTION AT A GLANCE

In this section we introduce a framework to discuss observations and experiments by summarizing four well-known theories of reconnection. The first two are the steady-state MHD theories of slow and fast reconnection, respectively. The third is a theory for spontaneous, time-dependent MHD

Table 1 Table of frequently used quantities, including formulae and values in cgs units. Definitions are standard; τ_e is taken from Braginskii (1965). The quantity λ is the Coulomb logarithm, given by Braginskii as $23.4 + 1.15 \log (T_e^3/n_e$ for $T_e < 5.7 \times 10^5$ K and $25.3 + 1.15 \log T_e^2/n_e$ for $T_e < 5.7 \times 10^5$ K

Symbol	Quantity	Formula	Value
τ_e	Electron collision time	$\frac{3}{\sqrt{32\pi}} \frac{m_e^{1/2}(kT_e)^{3/2}}{\lambda e^4 n_i}$	$\frac{2.9\times10^{-2}}{\lambda/10} T_e^{3/2} n_e^{-1}$ s
ω_{ce}	Electron gyrofrequency	$\frac{eB}{m_e c}$	$1.8 \times 10^7 B$ s^{-1}
ω_{cp}	Proton gyrofrequency	$\frac{eB}{m_p c}$	$9.6 \times 10^3 B$ s^{-1}
ω_{pe}	Electron plasma frequency	$\left(\frac{4\pi n_e e^2}{m_e}\right)^{1/2}$	$5.6 \times 10^4 n_e^{1/2}$ s
ω_{pp}	Proton plasma frequency	$\left(\frac{4\pi n_p e^2}{m_p}\right)^{1/2}$	$1.3 \times 10^3 n_p^{1/2}$ s
δ_e	Electron skin depth	$\frac{c}{\omega_{pe}}$	$5.4 \times 10^5 n_e^{-1/2}$ cm
δ_p	Proton skin depth	$\frac{c}{\omega_{pp}}$	$2.3 \times 10^7 n_p^{-1/2}$ cm
σ	Electrical conductivity	$\frac{\omega_{pe}^2 \tau_e}{4\pi}$	$7.3 \times 10^6 T_e^{3/2} (10/\lambda)$ s
η	Magnetic diffusivity	$\frac{c^2}{4\pi\sigma} = \frac{\delta_e^2}{\tau_e}$	$\frac{9.9\times10^{12}}{T_e^{3/2}} (\lambda/10)$ cm^2 s^{-1}
v_A	Alfvén speed	$\frac{B}{\sqrt{4\pi m_p n_p}} = \omega_{ci}\delta_i$	$2.2 \times 10^{11} B n_p^{-1/2}$ cm s^{-1}
S	Lundquist number	$\frac{L v_A}{\eta} = \frac{L}{\delta_i}(\omega_{ce}\tau_e)$	$2.3 \times 10^{-2} L B T_e^{3/2} n_e^{-1/2} (\lambda/10)^{-1}$

reconnection initiated by an instability called the tearing mode. The fourth applies to plasmas that are collisionless and so cannot be described by MHD. For more extensive discussions of these theories, and open research issues surrounding them, see Section 5. Some important physical quantities used throughout this review are given in **Table 1**.

2.1. Steady State Reconnection

Parker (1957) and Sweet (1958) were the first to formulate magnetic reconnection as a local problem in which the inflow of plasma was connected with an outflow from the diffusion region. **Figure 1** depicts their model.

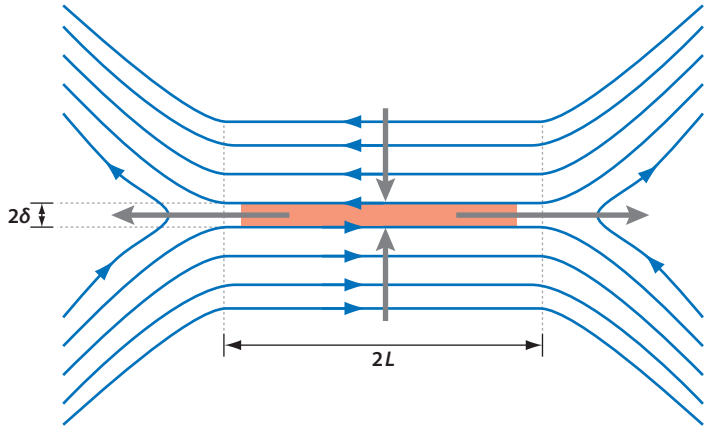

Figure 1

Sketch of magnetic field geometry in Sweet-Parker reconnection. Oppositely directed magnetic fields are brought together over a length $2L$ and reconnect in a diffusion layer of width 2δ.

Two oppositely directed magnetic fields, $\pm B$, in a plasma with density ρ and conductivity σ are carried toward the neutral line at speed v_{in} over a characteristic distance $2L$. There is a null point at the center of the configuration and a layer of width 2δ in which the field reconnects. Reconnected field and plasma are expelled at speed v_{out}. The system is assumed to be in a steady state. The Sweet-Parker theory predicts the reconnection rate v_{in} and establishes the basic energetics and geometry of the reconnection region based on the following three principles: (*a*) The outflow speed is the Alfvén speed given in Gaussian units by $v_A \equiv B/\sqrt{4\pi\rho}$. This follows from assuming magnetic energy is converted to plasma kinetic energy through resistive heating, which raises the pressure, and through the magnetic tension force associated with the sharp bend in the fieldlines near the X-point. Both effects accelerate the fluid to roughly v_A. (*b*) Mass is conserved. For an incompressible flow, $v_{in}L = v_A\delta$. (*c*) The electric field $\boldsymbol{E}$, given by the resistive MHD form of Ohm's Law as

$$\boldsymbol{E} = -\frac{\boldsymbol{v} \times \boldsymbol{B}}{c} + \frac{\boldsymbol{J}}{\sigma}, \tag{1}$$

is perpendicular to the plane of the flow and must be constant in a steady state. It is primarily inductive everywhere except near the X-point, where it is primarily resistive. This gives $v_{in}B/c \sim J/\sigma$. Estimating J from Faraday's Law, $J \sim cB/(4\pi\delta)$. Introducing the magnetic diffusivity $\eta \equiv c^2/(4\pi\sigma)$ and using relations (*a*)–(*c*) gives

$$\frac{\delta}{L} = \frac{v_{in}}{v_A} = S^{-1/2}, \tag{2}$$

where the Lundquist number S (see **Table 1**) is the ratio of the global Ohmic diffusion time $\tau_{diff} \equiv L^2/\eta$ to the global Alfvén time $\tau_A \equiv L/v_A$.

Owing to Faraday's Law, there is a close connection between the reconnection velocity $v_{in} = v_{rec}$ and the opening angle of the field. If we assume the inflow is along $\hat{x}$ and the outflow is along $\hat{z}$, then

$$\tan\theta \equiv \frac{B_x}{B_z} = \frac{v_{in}}{v_{out}} = \frac{v_{rec}}{v_A}, \tag{3}$$

so the reconnection rate increases with increasing θ. For Sweet-Parker reconnection, $\tan\theta \sim S^{-1/2}$. From Equation 2, the reconnection rate is inversely correlated with the current sheet length, $v_{in} \propto L^{-1/2}$.

The energetics of Sweet-Parker reconnection can be estimated from Equation 2. The Poynting flux into the layer, $v_{in}LB^2/4\pi$, is of the same order as both the kinetic energy flux out, $\rho v_A^3\delta/2$, and the Ohmic dissipation rate $J^2\delta L/\sigma$ inside the layer. Thus, roughly equal amounts of energy go into accelerating thin Alfvénic jets and heating the electrons.

Most astrophysical systems have very large S. In such systems, the Sweet-Parker reconnection rate is very slow. This difficulty is not easily overcome. The resistive layer must be thin because that is the only way to make the current density large enough to dissipate the incoming magnetic energy. But the resistive layer width is also the width of the outflow, which means that the mass flux out of the layer is very small. This, in turn, limits v_{in}. All theories that predict faster reconnection rates must in one way or another address these problems.

As simple as this model is, its main features are common to most reconnection theories. There is a small dissipation region, strong outflows, and hot electrons.

Sweet-Parker reconnection provides another acceleration mechanism worth remarking on: Near the X-line, particles can be freely accelerated by the electric field parallel to the reconnection plane (Friedman 1969, Bulanov & Sasorov 1975, Zweibel & Bruhwiler 1992). If the reconnection region extends for a distance D, the maximum possible energy gain is ZeED, which can be large, but most particles drift away from the X-line before reaching this energy. Particle energy

spectra produced by this mechanism do not fit astrophysical spectra very well, which has diminished interest in this mechanism (see, however, Sections 5.3.2 and 5.6, and Zenitani & Hoshino 2007).

2.2. Fast Steady-State Reconnection

Sweet-Parker reconnection is slow because all the fluid brought into the reconnection region must flow out through a thin, resistive channel. Petschek (1964) realized that reconnection would be faster if the resistive layer were short and most of the incoming fluid did not pass through it, but instead was redirected by standing shock waves, as shown in **Figure 2**.

According to the continuity argument given in Section 2, if the length L is replaced by a shorter length L', the reconnection rate increases by $\sqrt{L/L'}$. Petschek derived a family of solutions with progressively smaller L', down to a limit of $L(8 \ln S/\pi\sqrt{S})^2$. The corresponding maximum reconnection rate is $v_A(\pi/8 \ln S)$. This upper limit is generally a few percent of the Alfvén speed, fast enough to account for most astrophysical phenomena. Petschek's theory is widely cited in support of fast reconnection.

Petschek's theory was based on analytical arguments. Attempts to verify it through numerical MHD simulations show that this type of reconnection does not develop by itself and, if imposed as an initial condition, is not stable, unless the magnetic diffusivity η increases near the X-point. From an intuitive point of view, one can see that the larger η is, the faster the fieldlines are reconnected in the resistive layer, and the faster new fieldlines can be brought in. If η has a maximum at the X-point and rapidly decreases away from it, a large reconnection angle can be formed (see Equation 3) and reconnection is sped up.

A general feature of Petschek-like models is that, in contrast to the Sweet-Parker model, most of the energy is converted to the ion kinetic energy of the outflow and, if shocks are present, to heat, with relatively little energy going into resistive heating of the electrons.

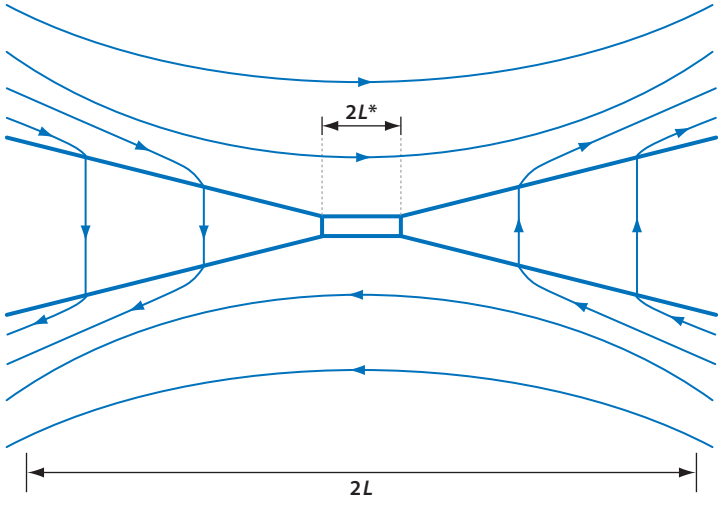

Figure 2

Sketch of magnetic field geometry for Petschek's fast magnetohydrodynamic reconnection model. The current sheet is short, and most of the fluid never reaches it, being turned instead by two pairs of slow mode shocks.

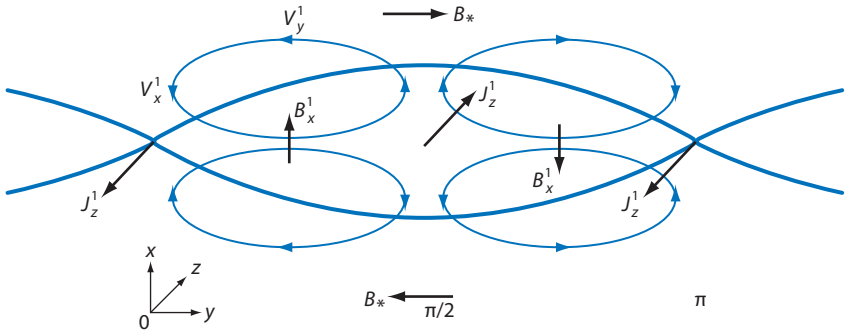

Figure 3

Sketch of magnetic field geometry for the tearing mode. There is a large, nearly constant guide field perpendicular to the page. The sheared component has reconnected, forming a chain of magnetic islands. Resistive effects are large only near the X-points.

2.3. Spontaneous Reconnection

The Sweet-Parker and Petschek models describe steady-state reconnection, but do not address the circumstances under which it occurs. A new ingredient was added by Furth, Killeen & Rosenbluth (1963), who showed that a magnetic field can be unstable to small perturbations, called tearing modes, which reconnect the fieldlines. An example of a tearing mode is shown in **Figure 3**. There is a strong, nearly uniform component of field, called the guide field, perpendicular to the plane of the figure. Because the in-plane component B_y reverses at $x = 0$, the magnetic tension force that results from bending the fieldlines goes through zero, and resistivity competes with dynamics.

Instability requires a gradient in the current density, and the gradient length scale must be much less than the perturbation length scale k^{-1}. Otherwise, magnetic tension stabilizes the mode. It is found that the growth time of the most unstable mode is of order $\tau_A S^{3/5}$ and the width of the resistive layer relative to the global scale is of order $S^{-2/5}$. These dependences on S are similar to the Sweet-Parker scalings, according to which 3/5 and $-2/5$ are replaced by 1/2 and $-1/2$, respectively.

The energetics of the tearing mode was analyzed by Adler, Kulsrud & White (1980). They showed that the tearing mode reduces the magnetic energy, and that the driving energy comes from the unstable current gradient within the tearing layer. As in Sweet-Parker reconnection, the magnetic energy is transformed to ion flow energy and electron thermal energy.

As tearing progresses, the magnetic islands shown in **Figure 3** widen. Once the island width exceeds the resistive layer width, nonlinear $\boldsymbol{J} \times \boldsymbol{B}$ forces become significant. Exponential growth is replaced by linear growth, at a rate proportional to η (Rutherford 1973). During this very slow growth stage, the initially unstable current profile flattens. The mode saturates when the current profile has reached marginal stability.

Resistive instabilities can be modified by the same MHD forces that drive ideal instabilities. The resistive kink mode, like the ideal kink, is driven by an unstable current profile and is an example. Its growth time is of order $\tau_A S^{1/3}$, faster than the tearing mode, but still slow in most astrophysical systems. Like the tearing mode, the resistive kink makes a transition from exponential to algebraic growth once the island width reaches a finite value. But unlike the tearing mode, the resistive kink does not saturate. Instead, a current sheet forms and reconnection becomes fast (Waelbroeck 1989). This type of two-stage process is one way to achieve fast reconnection and can be considered a form of driven reconnection (Section 6.2).

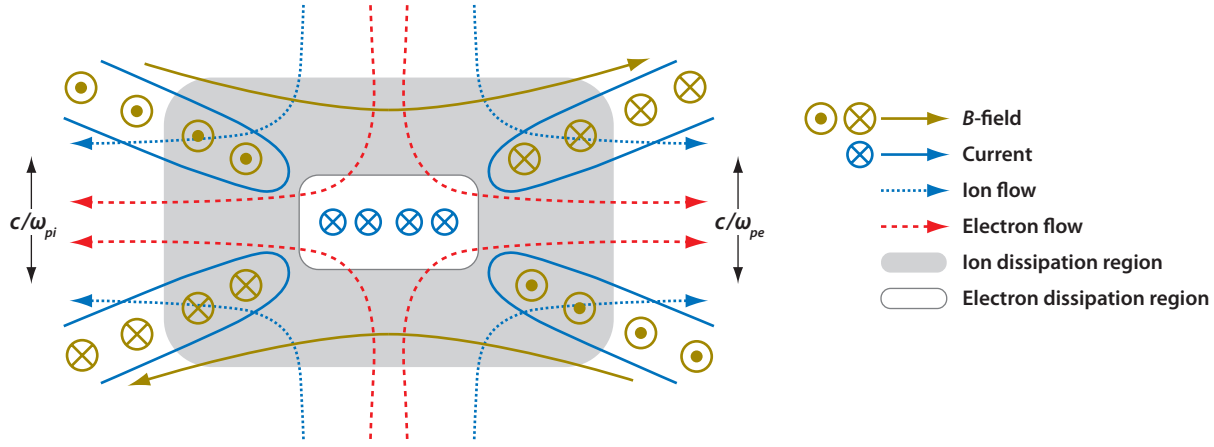

Figure 4

Sketch of magnetic field geometry in collisionless reconnection. The ions decouple from the electrons at a distance $\delta_i \equiv c/\omega_{pi}$ from the neutral line. The electrons continue flowing inward and the field is reconnected within the much thinner electron diffusion layer.

2.4. Collisionless Reconnection

Up to now, we have used the resistive MHD form of Ohm's Law, given by Equation 1 with **v**, fluid velocity. The meaning of Ohm's Law is that in a steady state, the Lorentz force on the electrons is balanced by frictional drag due to collisions. Thus, $\boldsymbol{v}$ is understood to be the electron velocity $\boldsymbol{v}_e$. Using the relation $\boldsymbol{J} \equiv (\boldsymbol{v}_i - \boldsymbol{v}_e)en_e$ (valid for singly charged ions in a quasineutral plasma) and assuming $\boldsymbol{v} \sim \boldsymbol{v}_i$, Ohm's Law can be written in a form that accounts for $\boldsymbol{v}_e \neq \boldsymbol{v}_i$:

$$\boldsymbol{E} + \frac{\boldsymbol{v} \times \boldsymbol{B}}{c} - \frac{\boldsymbol{J} \times \boldsymbol{B}}{en_e c} = \frac{\boldsymbol{J}}{\sigma}. \tag{4}$$

The $\boldsymbol{J} \times \boldsymbol{B}$ term in Equation 4 represents the Hall effect. When the Hall term dominates, the in-plane electron flow into and out of the reconnection region corresponds to an in-plane current. This differs from the Sweet-Parker and Petschek models, in which the current is entirely perpendicular to the reconnection plane. The situation is sketched in **Figure 4**.

Consider the out-of-plane ($\hat{y}$) component of Equation 4 near the magnetic X-point. It can be shown that the ion velocity $\boldsymbol{v}_i \sim \boldsymbol{v}$ approaches zero on scales below the so-called ion inertial length or ion skin depth δ_i (see **Table 1** and Equation 8). One can think of δ_i as the gyroradius of an ion moving at the Alfvén speed: $\delta_i = v_A/\omega_{ci}$. On scales $\delta < \delta_i$, $\boldsymbol{E}$ is supported by the Hall term or the resistive term (electron pressure can also play a role, but we ignore that for the time being).

The out-of-plane component of the Hall term can be written in terms of Ampere's Law as

$$\left(\frac{\boldsymbol{J} \times \boldsymbol{B}}{en_e c}\right)_y = \frac{\boldsymbol{B} \cdot \nabla \boldsymbol{B}_y}{4\pi en_e}. \tag{5}$$

Equation 5 shows that the in-plane current generates an out-of-plane field, B_y. We can derive the spatial form of B_y from the behavior of J_x and J_z near the X-point. Because J_x represents electron inflow and J_z represents electron outflow, $J_x \propto x$ and $J_z \propto -z$. From Ampere's Law, $B_y \propto xz$, that is, the out-of-plane field has a quadrupole pattern.

When do we expect the Hall effect to be important in reconnection? Recall that in MHD reconnection, the electric field is inductive outside the reconnection region and resistive within it. Because the Hall effect takes place on scales less than δ_i, we expect Hall reconnection when

$\delta_{SP} < \delta_i$. Using Equation 2, we find

$$\frac{\delta_{SP}}{\delta_i} = \left(\frac{L}{\lambda_{mfp}}\right)^{1/2} \left(\frac{m_e}{m_i}\right)^{1/4}, \tag{6}$$

where λ_{mfp} is the electron mean free path; we have assumed $T_e = T_i$, $v_A \sim v_{thi}$ ($\beta \sim 1$ in the reconnection layer), and $\eta_\perp \sim 2\eta_\parallel$ owing to the magnetic field (Yamada et al. 2006). Equation 6 shows that the Hall effect should become important in reconnection when the length of the current sheet is comparable to the electron mean free path. For that reason, Hall reconnection is sometimes called collisionless reconnection.

Under certain conditions, Hall reconnection proceeds quite fast, at about 0.1 v_A. The reasons for this, and the relevance of Hall reconnection in astrophysics, are subjects of current research and are discussed more extensively in Section 5.2.

3. RECONNECTION OBSERVED

In the models summarized in Section 2, reconnection changes magnetic topology and converts magnetic energy to particle energy: the electrons through Ohmic heating and the ions through acceleration of Alfvénic jets. The particle energization layer is thin, but the topological rearrangement is global. Some of these signatures of reconnection have now been observed in space and astrophysical plasmas.

Solar flares inspired much of the early research on reconnection. Historically, flares were defined by localized, sudden brightening of the chromosphere in Hα. Zeeman measurements of the line-of-sight photospheric magnetic field showed the presence of both positive and negative polarities, suggesting that the overlying coronal fieldlines formed closed loops. A prominence often erupted in conjunction with the flare. Radio emission from the high corona showed evidence for outward traveling disturbances. For a review of flare theory and observations during this early period, see Pneuman (1981).

In the past three decades, a series of space observatories, including SMM, Yohkoh, SOHO, TRACE, RHESSI, and Hinode, expanded the wavelength coverage of flares to include EUV, X-rays, and γ-rays, and provided imaging and spectroscopy at high spatial and temporal resolution. Similar advances have occurred in radio facilities and in magnetic field measurement techniques. The result is a richer picture of flare phenomenology, aspects of which have been reviewed by Bastian, Benz & Gary 1998; Ramaty & Mandzhavidze 2000; Priest & Forbes 2002; Dennis, Hudson & Krucker 2007; Murphy 2007; and Hudson 2009.

The Hα emission is now known to be accompanied by X-rays at tens to hundreds of kilo eletron volts, μ-wave emission, and, in some flares, γ-ray emission. The hard X-rays are bremsstrahlung from electrons with energies in the tens to hundreds of kilo electron volt range. The μ waves are gyrosynchrotron radiation from the same electrons, whereas the Hα is excited by the fast electrons as they slow down in the chromosphere. The γ-rays result from $e^\pm$ annihilation, neutron capture on protons, and the decay of excited nuclear states, and they are evidence that ions are accelerated at least to tens of Megaelectron volts. The particle energy spectra are nonthermal and typically fit by broken power-laws with spectral indices in the range of 4–6.

Most of the emission comes from the chromospheric footpoints of the coronal loops, where the high gas density makes the interaction time short. However, the presence of μ-wave hotspots at the loop tops, as well as other morphological evidence, suggests that the particles are accelerated in the corona. The emission is typically sustained for hundreds to thousands of seconds, but varies on timescales as short as several microseconds. This could be due either to an intermittent acceleration mechanism or to propagation effects (Zweibel & Haber 1983). It is estimated that

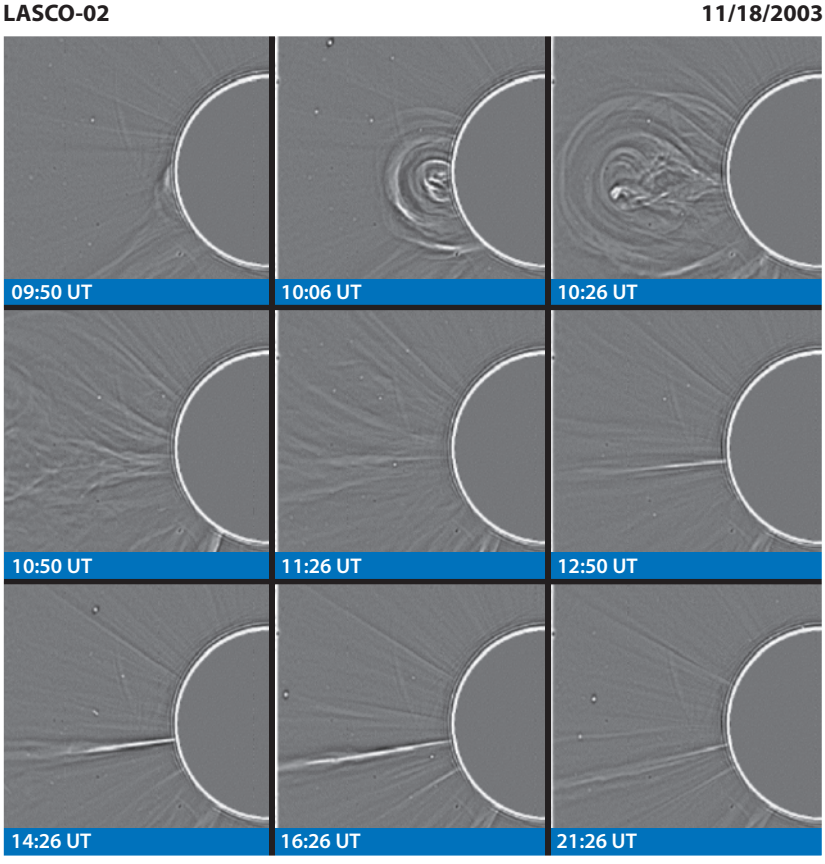

Figure 5

Time sequence of coronal density images made with the LASCO coronagraph on SOHO showing apparent expansion and detachment of a loop structure over a period of hours. The field of view is 1.5 to 6 $R_\odot$. From Lin et al. (2005).

an energy of 10^{31}–10^{32} ergs is released into fast particles over the duration of a large flare. This corresponds to 10^{36}–10^{38} particles and is comparable to the number of particles in a typical flare loop rather than at a single small reconnection site (Aschwanden 2002, Fletcher & Hudson 2008).

The morphology of some flares suggests reconnection. Cusp or X-shaped structures are seen at the tops of flare loops (Masuda et al. 1994). Positive temperature gradients have been measured at some loop tops, suggesting that the reconnection site moves upward and the post reconnection loops cool (Tsuneta 1996). An example of the evolution of a loop system is shown in **Figure 5**.

Ciaravella & Raymond (2008) found evidence for a postflare vertical current sheet tens of thousands of kilometers wide that persisted for many hours. The reconnection picture is supported by the observed separation with time of the Hα footpoints, which could be interpreted as successive energy release within a series of nested loops. Forbes & Priest (1982) proposed a method for estimating the reconnection rate based on the separation rate of the Hα footpoints. Implementation of the method yields speeds from tens to as high as 200 km s^{-1} (Jing et al. 2005; Lee, Gary & Choe 2006). A sense of how dynamical these processes are can be obtained from movies such as those made from TRACE data, available at **http://trace.lmsal.com/POD/TRACEpod.html**.

Flares occur in regions of high magnetic stress, and the magnetic energy is reduced by flaring. Although traditional magnetograms measure only the line-of-sight component (or at disk center, the radial component) of magnetic field, vector magnetograms measure all components (Lites 2000). It is possible to extrapolate the field into the outer atmosphere and estimate the magnetic energy in the region, provided one makes additional assumptions. Most such reconstructions are based on the principle that $\boldsymbol{B}$ should be force free: $\boldsymbol{J} = \alpha \boldsymbol{B}$, which implies $\boldsymbol{J} \times \boldsymbol{B} \equiv 0$. This assumption is well justified by the low plasma β of the corona, its large-scale height, and the short Alfvén transit times of coronal structures. For a discussion of extrapolation of photospheric field measurements see Schrijver et al. (2008). In cases where the preflare and postflare magnetic energies can be measured and compared with the energy in fast particles, it is found that the magnetic energy decrease during the flare is of the same order as the energy in fast particles (and also comparable to the energy associated with mass ejection; Emslie et al. 2004).

A subtle aspect of the connection between magnetic topology and flare energetics was pointed out by Aly (1984) and Sturrock (1991). It is well known that the minimum energy state consistent with a given photospheric flux distribution is the current free or potential state ($\boldsymbol{B} = \nabla\Phi$, with $\nabla^2\Phi \equiv 0$), in which all the fieldlines are closed (the dipole field is an example). Aly and Sturrock showed that the maximum energy state is completely open and current free except on thin sheets separating regions of opposite polarity, thus completely opening the field costs energy rather than releasing it. Implications of this for the energetics of coronal mass ejections are reviewed by Low (1996).

The distribution of flare energy emission rates follows a power-law over several decades (Dennis 1985, Nita et al. 2002, Veronig et al. 2002, Su et al. 2006). Lu & Hamilton (1991) suggested that this could be the signature of an avalanche-like process, where individual reconnection events have some probability of triggering others (see also Charbonneau et al. 2001). The power-law index is tantalizingly close to the critical value of 2, above which the energy release rate is dominated by the smallest events. This supports the idea that the solar corona is heated by small reconnection events, or nanoflares (Parker 1990, Klimchuk 2006; but see Aschwanden 2008).

In summary, flares show many of the signatures of magnetic reconnection—fast particles, topological changes in the magnetic field, evidence for release of magnetic energy—but they show them on unexpectedly large size scales and short timescales. It has long been known that the standard models of steady-state or resistive reconnection cannot account for the short energy release times seen in flares. The morphology suggestive of reconnection is on a scale many orders of magnitude larger than expected from standard reconnection models. The number of fast particles is much larger than could reasonably be accelerated in a single reconnection region, and the power-law spectra argue for energization mechanisms other than simple Ohmic heating or bulk acceleration of jets [the energy of a proton moving at the Alfvén speed is 0.25 MeV $(B/100G)^2(10^9/n)$]. Possible resolutions of these problems include a substantial MHD energy release process in addition to the resistive process, reconnection-driven turbulence that spreads through the loop and accelerates particles, and/or multiple reconnection sites, possibly triggered sequentially. Reconnection models must also accommodate tying of the fieldlines at the photosphere; see Sections 5.4 and 6.1.

Although the Sun is close by astrophysical standards, it is still probed primarily through remote sensing. The interaction between the terrestrial magnetosphere and the magnetic field of the solar wind is the nearest natural environment in which reconnection can be studied in situ. One could imagine that the wind is simply deflected around the magnetosphere as though it were an impermeable obstacle, but this does not happen. Instead, the two systems of fieldlines become attached by reconnection, and the terrestrial fieldlines are swept back into a tail. In addition to the more or less steady reconnection required to maintain this configuration, explosive outbursts of energy, probably powered by reconnection, occur sporadically in the magnetotail. A number of

spacecraft, including ISEE, *Polar*, *Geotail*, ACE, *Wind*, *Cluster*, and *THEMIS*, have been used to measure electric and magnetic fields and particle spectra in the solar wind and magnetosphere in situ, and obtain reconnection data complementary to what can be gleaned from solar flares.

The Alfvénic jets that carry plasma and magnetic fields away from the reconnection region (see Section 2) have been detected in the solar wind (Gosling et al. 2005, 2007) and provide valuable information on the overall magnetic geometry. The jets are centered on reversals of the in-plane components of the magnetic field (there is generally also a field component normal to the plane of the flow). Referring back to the Sweet-Parker model, Equation 2 shows that the field reverses within an angle θ_r of order δ/L. The reconnection rate can be written in terms of θ_r as $v_{in} \sim v_A \sin \theta_r$. In order for the jets to be well sampled, the flow speed must be measured at intervals shorter than the time it takes the jet to sweep over the spacecraft. This favors detection of broad outflows signifying fast reconnection. The events detected originally (Gosling et al. 2005) were of this type, whereas later observations at higher time cadence showed a large number of thin outflows accompanying reconnection at a slower rate (Gosling et al. 2007). Although the strong selection bias in favor of broad outflows makes it difficult to measure the true distribution of reconnection rates, it is gratifying that the outflows, accompanied by the expected magnetic field reversals, are seen at all.

In situ measurements by a single spacecraft cannot distinguish between variations with position and variation with time. A remarkable opportunity to study reconnection in the solar wind occurred when the ACE, Cluster, and Wind spacecraft trajectories were separated by only a few hundredths of an AU $\sim 10^6$ km over a window of approximately 3 h (Phan et al. 2006). The magnetic field data and particle velocity measurements obtained by each spacecraft during this time could be interpreted by a model in which steady reconnection at about 0.03 v_A occurred for at least 2.5 h, with inflow scale L at least 2.5×10^6 km (or 390 R_E; this lower limit is based on the separation of the spacecraft, all of which were located within the same outflow). Similar reconnection outflows were also seen earlier at the terrestial magnetopause (Paschmann et al. 1979, Eriksson et al. 2004).

In the magnetosphere, measurements of the reconnection region were analyzed by Mozer, Bale & Phan (2002). These researchers found evidence for a quadrupolar out-of-plane magnetic field in the electron diffusion region. This is a signature of collisionless reconnection (Sections 2.4 and 5.2). More recently, Phan et al. (2007) have reported a more complete picture of a reconnection event in the terrestrial magnetosheath. In addition to measuring the reconnection electric field and the quadrupolar magnetic field, they measured the reconnection rate ($v_R/v_A \sim 0.07$) by comparing the measured inflows and outflows. Furthermore, they found evidence for an electron diffusion region inside the ion diffusion region, which is in agreement with recent simulations and with laboratory data from MRX (see Section 4).

Decoupling of the electrons and ions from the magnetic field, as well as spatially localized, low-frequency turbulence, was seen in the diffusion region measurements analyzed by Mozer, Bale & Phan (2002), whereas two-fluid reconnection in a turbulent environment was identified by Retinò et al. (2007). Depending on the nature of the turbulence, it can be a source of anomalous resistivity (Section 5.3.1), cause particle acceleration and heating (Section 5.3.2), and increase the reconnection rate by creating multiple reconnection sites and modifying the outflow from the diffusion region (Section 5.7). Thus, direct evidence for turbulence is encouraging.

In summary, the heliosphere and terrestrial magnetosphere are rich environments for studying collisionless reconnection in natural plasmas. Because the ratios of important plasma length scales, such as ion skin depth, ion gyroradius, and electron mean free path to the global size of the system, are very different from their astrophysical values, it is important to understand the coupling between local and global scales in reconnection.

The evidence for reconnection in remote astrophysical systems is less direct than in the heliosphere, but we argue on theoretical grounds that it is ubiquitous. Reconnection must occur in

any magnetic field sustained by a dynamo because topological changes in the field are essential to dynamo activity. As there is convincing evidence for dynamos in stars, galaxies, and possibly accretion disks, reconnection must occur throughout these systems.

Reconnection is often assumed to be the energy source underlying flares and outbursts of all types. Stellar activity is magnetically driven, and stellar flares are similar to solar flares (Rosner et al. 1985; Haisch, Strong & Rodono 1991; Güdel 2004). The strongly magnetized neutron stars classed as anomalous X-ray pulsars and as soft gamma repeaters also flare, SGR 1806-20 being a particularly dramatic example (Kaspi et al. 2003, Hurley et al. 2005), pointing to rapid release of magnetic energy, possibly through reconnection (Thompson & Duncan 1995, Lyutikov 2003, Schwartz et al. 2005). Galeev, Rosner & Vaiana (1979) suggested that magnetically structured coronae similar to the solar corona would form in the hot accretion disks surrounding black holes, and that the observed hard X-ray variability of such disks could be due to flares powered by reconnection (Miller & Stone 2000). Inoue, Totani & Ueda (2008) provided indirect support for this idea based on the similarity between the power-law electron spectra inferred for active galactic nuclei and in solar flares.

Reconnection has consequences besides its role in outbursts. It has been invoked as a heat source in warm, ionized interstellar gas (Reynolds, Haffner & Tufte 1999). It vies with other dissipation mechanisms to determine the saturation level and other properties of instabilities such as the magnetorotational instability (Fromang et al. 2007) and shear flow instabilities (Palotti et al. 2008). It controls the extent to which stars and accretion disks can remain magnetically connected, as is necessary to transfer angular momentum by magnetic torques (Uzdensky, Konigl & Litwin 2002). Similarly, it determines how efficiently magnetic loops transport angular momentum within disks (Goodman & Uzdensky 2008). Differential electron and ion heating during reconnection could help to maintain a temperature difference between these species in collisionless systems such as accretion disks surrounding compact objects. It may be responsible for the acceleration of high-energy particles, either by DC electric fields or in reconnection-generated turbulence, in disks, extragalactic radio sources, and interstellar and intracluster gas.

Given the small expected volumes of reconnection regions, directly imaging reconnection in astrophysical settings is unlikely to ever be possible. Therefore, one of the goals of reconnection theory should be calculating the spectral signatures of reconnection. This might include a prediction for line profiles in the presence of many unresolved reconnection outflows and a particle distribution function of temperatures in a gas sporadically heated by reconnection. It would also require a kinetic model of reconnection that predicts the electron distribution function, so that ionization and excitation rates can be calculated correctly.

4. RECONNECTION IN THE LABORATORY

Magnetic reconnection has been studied in laboratory plasmas since the 1960s. In the early days laboratory experiments on reconnection were primarily conducted in short-pulsed (a duration of only a few microseconds) pinch-type experiments (Baum & Bratenahl 1974, Syrovastskii et al. 1973, Frank. 1974). These experiments were performed in the collision-dominated regime, and some interesting results were obtained, including identification of anomalous resistivity in the less collisional plasmas (Bratenahl & Yeates 1970). Two decades ago, more systematic experiments were carried out by Stenzel & Gekelman (1979) in a less collisional regime with a strong guide field. Although their experiment did not replicate a space-relevant plasma in which global plasma characteristics are described by MHD, their experiment was noteworthy in studying wave-related physics mechanisms in the reconnection region. They measured the local structure of non-MHD features of the reconnection region and found the relationship between the reconnection rate

and wave turbulence. However, one of the most important questions in reconnection, how the diffusive neutral sheet is formed in an MHD plasma with $\delta_i \ll L$ and $S \gg 1$, was not answered because the conditions for an MHD plasma were not satisfied outside the reconnection region in this setup.

In current carrying toroidal plasmas for fusion research, magnetic fields generated by internal plasma currents can effectively confine high-pressure plasmas by generating stable compressing (pinch) forces. In these systems, toroidal currents are induced to heat and confine the plasma. The tokamak, reversed field pinch (RFP), spheromak, and field-reversed configuration (FRC) belong to this category of confinement mechanism. In these plasmas reconnection plays a major role in forming the basic equilibrium configuration as well as in self-organization processes of their discharges. Although all these configurations generate self-pinching poloidal fields, toroidal fields are supplied differently: In tokamaks a strong field is supplied externally (Wesson 1987), whereas the toroidal field of the RFP is created by the combined effects of internal currents and a small external toroidal field (Taylor 1986), which is much weaker than that of tokamak. In a spheromak, which does not have an external toroidal field, the toroidal field is solely created by internal plasma current (Yamada et al. 1981, Bellan 2000). There is a notable common feature in all these configurations: Plasma constantly tends to relax into a more quiescent state through global magnetic self-organization, which involves magnetic reconnection.

In these current-driven fusion plasmas, the current configuration changes often dynamically, requiring rapid magnetic reconnection. Generally, magnetic reconnection occurs through 3D events, and extensive studies have been carried out to investigate the dynamics of this self-organization phenomenon. Sawtooth relaxation of tokamak plasma, which represents a cyclical change of the electron temperature profile, provides a good example of magnetic reconnection. During the sawtooth relaxation event, accompanied by rapid flattening of the electron temperature profile, the average pitch of the fieldlines changes suddenly as the fieldlines break and rearrange themselves to form a new topological profile. In the RFP and spheromak plasmas, a sudden rearrangement of fieldlines on an inner flux surface can trigger another rearrangement in the outer flux surfaces, signifying a global magnetic relaxation event.

4.1 Reconnection in Sawtooth Relaxation

A tokamak plasma is regarded as consisting of nested flux surfaces of axisymmetric toroidal shape, where T_e is assumed constant because of the large heat conductivity of high-temperature electrons along the magnetic field lines. The MHD stability of a tokamak plasma is determined by the safety factor q, which represents the inverse of the rotational transform of a toroidal magnetic configuration (Wesson 1987). In the large aspect ratio limit, q is approximated by aB_T/RB_p, where B_T, B_p, a, and R are the toroidal field, poloidal field, minor radius, and major radius, respectively. A peaked T_e profile in a tokamak generally tends to generate a more highly peaked current profile because of a higher conductivity at the center of the plasma. The resultant strong peaking makes the plasma unstable against an MHD mode. A helical MHD kink instability develops near a resonant ($\boldsymbol{k} \cdot \boldsymbol{B} \equiv 0$) flux surface and the helically deformed plasma can induce magnetic reconnection near the $q = 1$ surface, as shown in **Figure 6**. Kadomtsev (1975) proposed that the reconnection event (crash) should produce a uniform current-density configuration with $q = 1$ and a flat electron temperature (T_e) profile, and that the evolution is cyclic.

Utilizing cyclotron resonance radiation from the electrons, which contains information about the local magnetic field and local electron temperature, electron cyclotron emission (ECE) diagnostic systems were developed to measure the T_e profile as a function of radial position. Because the predominant toroidal field B_T depends on position as $B_T \propto 1/R$, this diagnostic can provide the

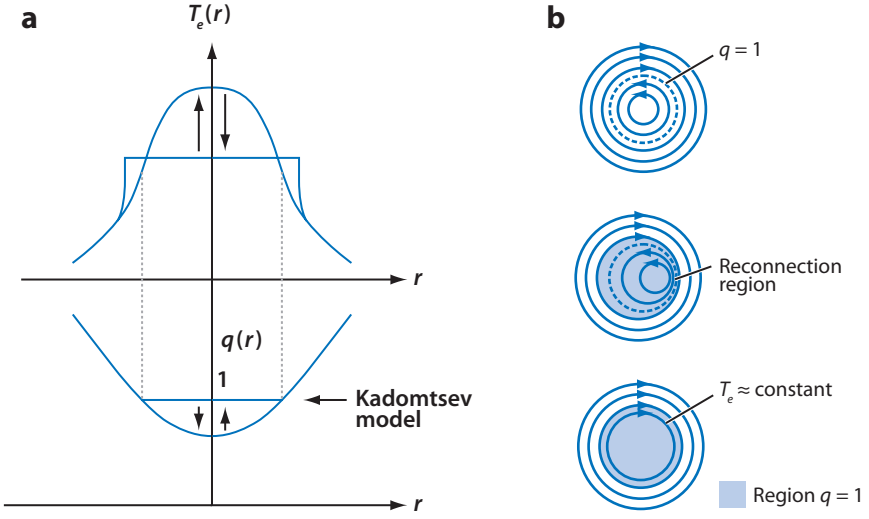

Figure 6

(*a*) Schematic view of changes of T_e and q profiles during sawtooth crash in a tokamak plasma. (*b*) Description of 2D Kadomtsev model in a toroidally cut plane; $m = 1$, $n = 1$ MHD instability develops near the $q = 1$ flux surface and induces magnetic reconnection (Kadomtsev 1975).

features of flux surfaces through electron temperature contours using an equilibrium code. The 2D electron temperature profile on a poloidal plane of the plasma was obtained utilizing a rigid body rotation model for a circular cross section tokamak, TFTR (Tokamak Fusion Thermonucler Reactor). The sawtooth crash phase, which takes 100–500 μs, was documented with this technique, as shown in **Figure 7** (Nagayama 1991, Yamada et al. 1994). By monitoring the change of T_e (transfer of heat) by color coding, fast electron heat transfer was measured. Just before the crash, a shrinking circular hot peak appears and a crescent-shaped flat island grows in the interior of the plasma.

Simultaneously, the motional Stark effect (MSE) diagnostic was employed (Levinton et al. 1993) to obtain directly the profile of the magnetic pitch angle, and hence the safety factor profile, $q(R)$, based on an equilibrium for a circular tokamak. With an assumption of axisymmetric flux surfaces, the measured fieldline pitch profile was translated into a radial profile of the rotational transform, or $q(R)$ profile, making use of tokamak equilibrium calculations by Yamada et al. (1994). During the crash phase, fast outward heat transfer across the $q = 1$ surface was observed. The observed fast heat flow was attributed to magnetic reconnection. The T_e profile inside the $q = 1$ radius becomes completely flat after the crash, which is consistent with Kadomtsev's model (Kadomtsev 1975).

However, the measured q profiles indicate that the central q value increases by 5%–10%, typically from 0.7 to 0.75, during the sawtooth crash phase but does not relax to unity, in disagreement with the prediction of Kadmotsev's 2D full reconnection model. The value of q_0 stays below unity throughout the sawtooth cycle. Because only fieldline breaking and rearrangement can make $q(R)$ change on such a short timescale, this measurement verifies that magnetic reconnection takes place even when the change of q is small. Similar changes in central q values were measured in the sawtooth crashes of circular cross section tokamaks by two groups [Soltwisch (1988); and Levinton et al. (1993), Yamada et al. (1994), and Nagayama et al. (1991, 1996)].

In summary, the recent extensive study of sawtooth relaxation in tokamaks to date has revealed the following two major points. Magnetic reconnection is often driven by an external ideal

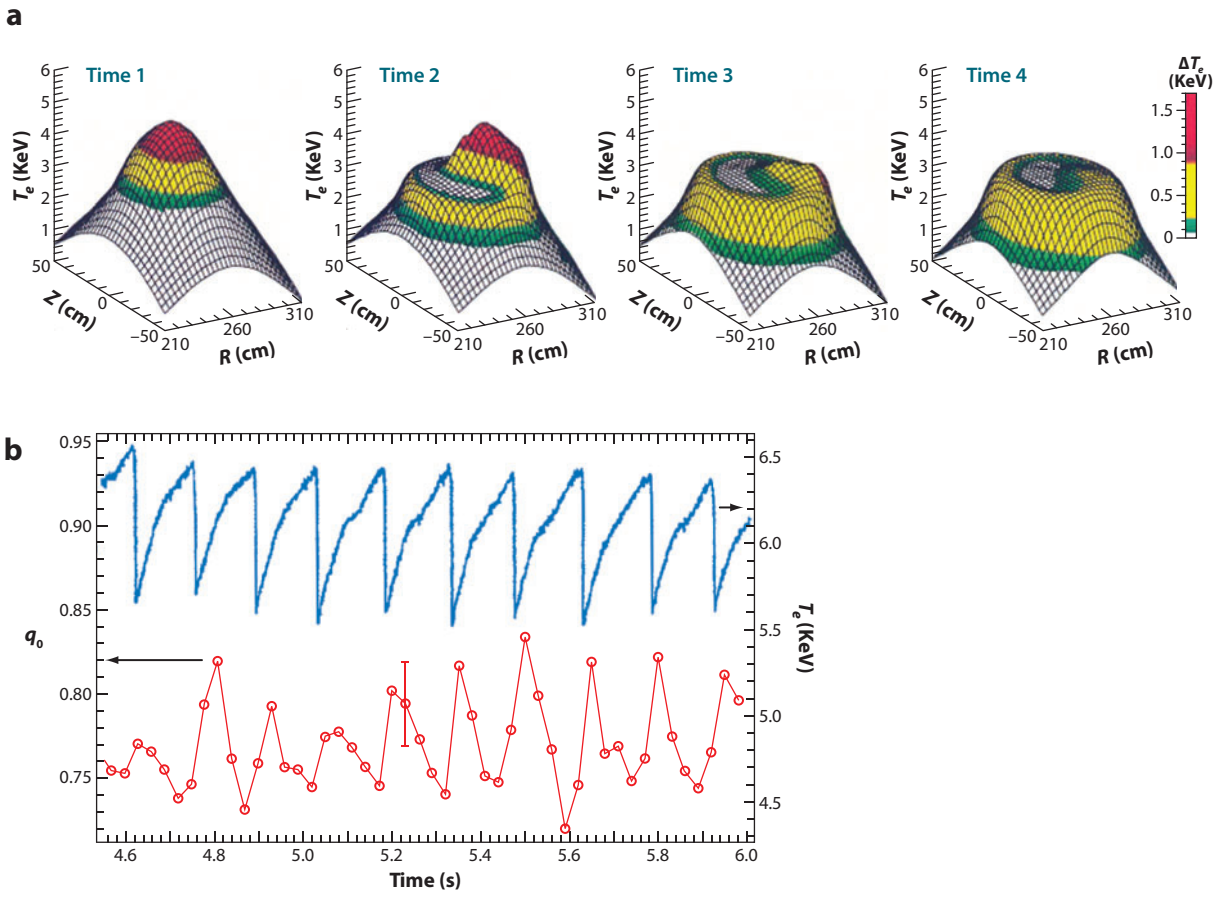

Figure 7

(*a*) 2D profile of T_e over the plasma cross section at four times during a reconnection event. The time interval between each frame is 120 μs. (*b*) Time evolution of peak electron temperature and measured central q value associated with sawtooth crash. From Yamada et al. (1994).

kink–type MHD instability, and the reconnection time is much faster than the Sweet-Parker time. This is expected because the Sweet-Parker model is only applicable to collisional plasmas and tokamak plasmas are collision free; $\lambda_{mfp} \ll R$. Heat diffusion transport can occur much faster than magnetic reconnection, namely on the timescale of electron heat conduction, leading to termination of kink modes and to inhibition of the Kadomtsev-type full reconnection process.

4.2 Magnetic Reconnection in Reversed Field Pinch and Spheromak Plasmas

RFP and spheromak plasmas are confined by a mixture of poloidal and toroidal magnetic fields. In contrast to tokamak plasmas, which are contained by the strong toroidal field, the strength of the internal magnetic field is comparable to that of the moderate external magnetic field both in RFP and spheromak plasmas. As argued by Taylor (1974, 1986), these configurations are generated by a process of magnetic self-organization in which a low β plasma settles into a state of minimum energy. Taylor also postulated that in the self-organization process, magnetic helicity, which is a measure of the "knottedness" and "twistedness" of a magnetic field (Woltjer 1958), should be

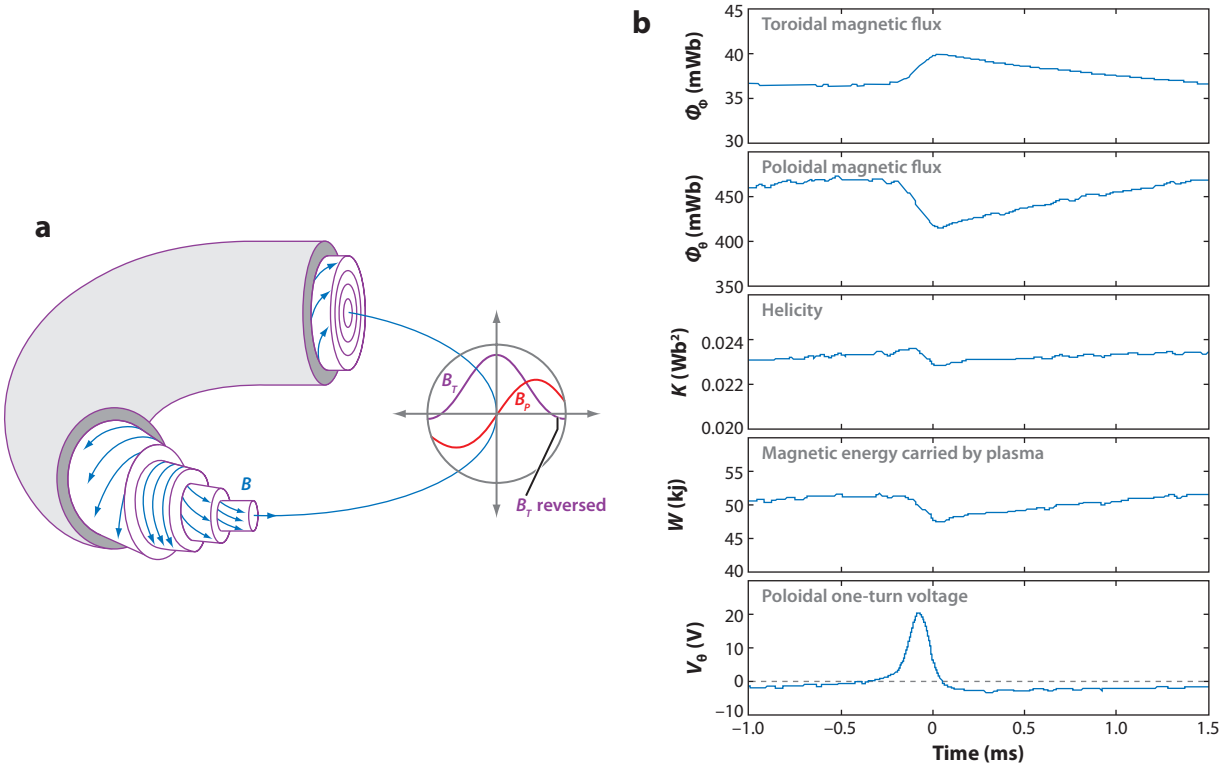

Figure 8

(*a*) Schematic of a reversed field pinch plasma configuration showing magnetic field lines, strongly sheared. B_T is toroidal field and B_P is poloidal field. Reconnection can occur at multiple surfaces, such as those indicated in the cutaway view of the toroidal plasma. The radial dependence of the poloidal and toroidal magnetic fields is plotted. From Sarff et al. 2005. (*b*) A discrete magnetic reconnection event in Madison Symmetric Torus. Shown are time evolution of toroidal magnetic flux, poloidal magnetic flux, helicity, magnetic energy carried by plasma, and poloidal one-turn voltage. (Ji, Prager & Sarff 1995.)

approximately conserved during relaxation events. Helicity is defined by

$$K \equiv \int \boldsymbol{A} \cdot \boldsymbol{B} dV, \tag{7}$$

where $\boldsymbol{A}$ is the magnetic vector potential and the integration is over the plasma volume V. If $\boldsymbol{B}$ is tangent to the surface of V, K is gauge invariant, and if the plasma is perfectly conducting, K is conserved. As shown in **Figure 8**, the RFP plasma is confined by a sheared magnetic field in which the magnetic field pitch changes its direction from the center (toroidal) to the edge of the plasma (poloidal). Magnetic reconnection also occurs during self-organization of a toroidally confined RFP plasma and can be both continuous and impulsive. When the current density profile becomes highly peaked, tearing modes develop, reconnecting magnetic field lines, and the plasma reorganizes itself rapidly to a new MHD equilibrium state. In this self-organization of magnetic field lines, a conversion of magnetic flux and energy from poloidal to toroidal occurs. **Figure 8*b*** presents time evolution of toroidal and poloidal fluxes together with magnetic helicity, magnetic energy, and one-turn poloidal voltage during a sawtooth relaxation event in an RFP.

In RFP plasmas, the role of local reconnection in the global relaxation phenomena has been experimentally studied (Ji et al. 1994, Sarff et al. 2005, Den Hartog et al. 2007). In the sheared

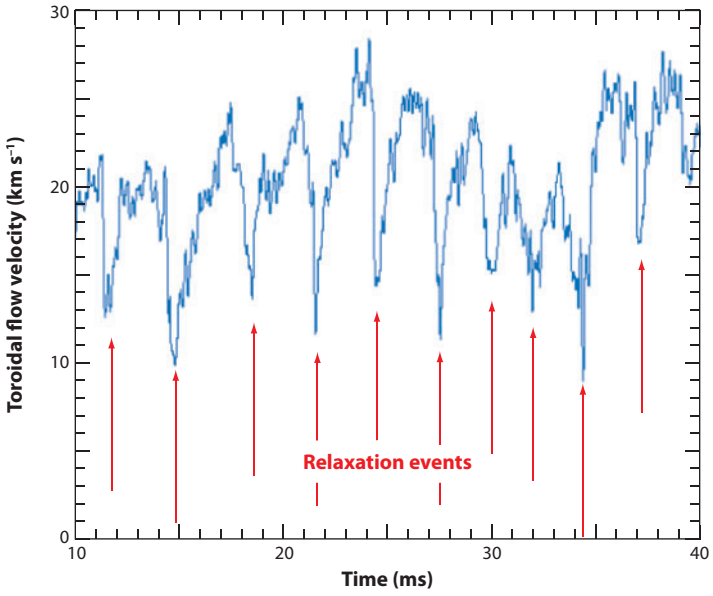

Figure 9

Rotational velocity of Madison Symmetric Torus plasma showing sudden reduction during reconnection (relaxation) events. Courtesy G. Fiskel and the MST Group (2008).

field line configuration, reconnection occurs at multiple radii in the plasma torus, with each radial location corresponding to a rational surface in which the safety factor is defined by m/n (m and n are poloidal and toroidal mode numbers, respectively). Often multiple reconnections occur suddenly and simultaneously, leading to a sudden global rearrangement of the magnetic field. One of the unique features of RFP relaxation is that the magnetic energy is converted to ion kinetic energy in a very short time. Both astrophysical and laboratory toroidal plasmas are observed to rotate in the toroidal direction. It is also known that the toroidal angular momentum is transported rapidly in the radial direction. During a reconnection event in Madison Symmetric Torus (MST), a sheared rotation of the plasma was observed to change suddenly during relaxation events as shown in **Figure 9**. Anomalous ion heating was also observed during this relaxation event. The exact causes of the anomalous transport are not yet determined. In the astrophysical situation, the force that transfers the angular momentum outward radially is believed to arise from flow-driven instabilities (Balbus & Hawley 1998). For RFP plasmas, it was found that the space and time varying fluctuations associated with the reconnection produce a large-scale Lorentz force that alters the rotation.

In spheromaks, relaxation events happen in a very similar way. But the rational surfaces of the spheromak plasma are more distinctively separated than those of RFP, so reconnection events in the center can be more isolated, as presented by Knox et al. (1986) and Ono et al. (1988).

4.3. Dedicated Experimental Research on Driven Magnetic Reconnection

A major objective of dedicated lab experiments for magnetic reconnection is to investigate the fundamental processes of magnetic reconnection by making a prototypical reconnection layer in a controlled manner. Their goal is not to simulate specific reconnection events in solar flares, the magnetopause, or accretion discs, but rather to provide key data to understand the fundamental

process of reconnection itself. In these experiments, a reconnection layer is created by driving oppositely directed fieldlines into the neutral sheet, thus generating a reconnection region in a controlled setting where plasma parameters can be varied. Magnetic field vector components can be measured simultaneously at a large number of points with use of fine-resolution probes in the reconnection region. By contrast, a space satellite can provide data only at finite number of points along the flight path. Current-carrying fusion plasmas provide typical examples of magnetic reconnection through self-organization processes, but it is very difficult to measure exact evolution of the magnetic reconnection layer profile because it is impossible to insert a probe inside. Thus, dedicated laboratory experiments can quantitatively cross-check theoretically proposed physics mechanisms and models by connecting local reconnection physics to global self-organization phenomena.

4.3.1. Controlled driven experiments: Magnetic Reconnection Experiment and Versatile Toroidal Facility. One form of controlled driven experiment is to program magnetic fieldline evolution after generating a quadrupole magnetic field configuration. The merging speed of oppositely directed fieldlines is determined by the external electric field provided by pulsed coil currents. This is the case in the MRX (Magnetic Reconnection Experiment) device, which was built at Princeton Plasma Physics Laboratory in 1995 by Yamada et al. (1997a,b). In MRX, reconnection is driven in a controlled manner with toroidal-shaped flux cores, which contain two types of coil windings in both the toroidal and poloidal directions, as seen in **Figure 10**. By pulsing programmed currents in the coils, two annular plasmas are formed inductively around each flux core, utilizing induced poloidal electric fields (Yamada et al. 1981, 1997a,b). After the plasmas are created, the coil currents are programmed to drive magnetic reconnection, generating a neutral sheet or a current layer to study the dynamics of the local reconnection layer. The evolution of the magnetic fieldlines can be seen by way of movies presented at the MRX Web site (**http://mrx.pppl.gov/mrxmovies**), which shows the time evolution of the measured flux contours of the reconnecting field. By monitoring these contours, the reconnection rate can be measured as a function of plasma parameters and compared with the Sweet-Parker model (Ji et al. 1998, 1999). In the past decade, extensive studies have been carried out to study many aspects of magnetic reconnection.

The analysis of MRX focuses on the coupling between local microscale characteristics of the reconnection layer and global properties such as external driving force and the evolution of plasma equilibrium. So far on MRX the local features of the reconnection layer have been extensively studied. The global plasma properties can be described by MHD with the ion gyroradius (1–5 cm) being much smaller than the plasma size ($R \sim 30$–50 cm). The overall initial geometry is axisymmetric (and hence 2D), but can be made nonaxisymmetric to study 3D characteristics of merging.

The Versatile Toroidal Facility (VTF) at the Massachusetts Institute of Technology (Egedal, Fasoli & Nazemi 2000) was built to explore fast magnetic reconnection with a strong guide field in the collisionless plasma regime, where the electron mean free path is much larger than the dimensions of the plasma. The VTF geometry is similar to that of MRX except for the much stronger guide field. The theoretical understanding gained from research on reconnection in the VTF was recently applied to interpretation of recent in situ measurements of the electron phase space distribution during reconnection in the deep terrestrial magnetotail. This is of particular relevance to the reconnection event observed by the Wind satellite. Electron current channels were detected near the X-point and their sizes were found to scale with the geometric mean of electron gyroradius and cusp field gradient scale (Egedal, Fasoli & Nazemi 2003). However, the current flowing in these layers is very small, so that the angle between the separatrices at the

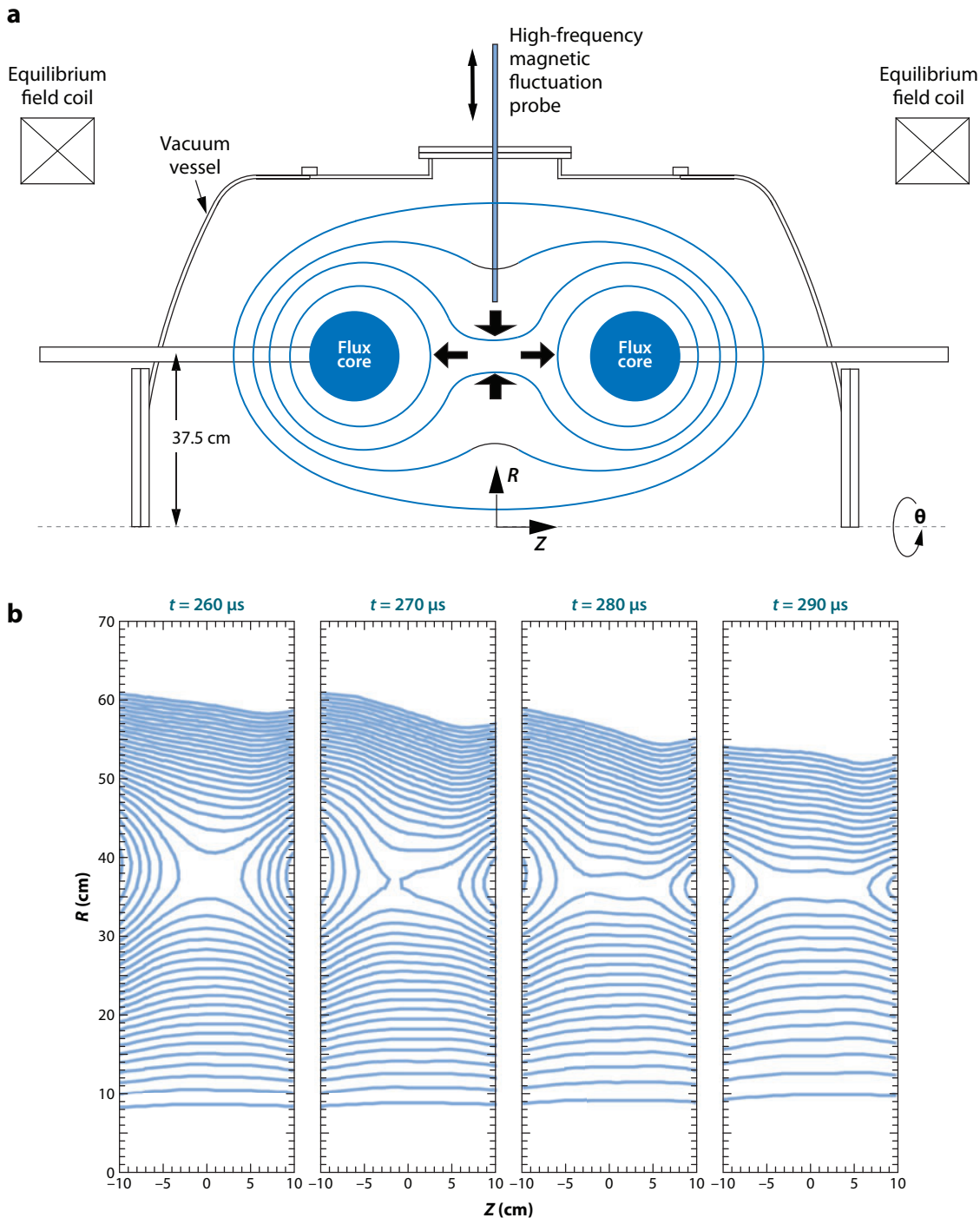

Figure 10

(*a*) Magnetic Reconnection Experiment apparatus with illustration of pull-driven reconnection by inductive coils. (*b*) Time evolution of flux contours during driven reconnection. Magnetic reconnection is demonstrated through measured fieldlines. In the low β plasma outside the neutral sheet, poloidal flux contours represent magnetic fieldlines. From Yamada 1997a,b.

X-point remains close to 90°, and the associated dissipation of magnetic energy is expected to be negligibly small. These features may not be compared straightforwardly with the numerical simulation results for reconnection where we expect a sizable amount of neutral sheet current.

4.3.2. Colliding spheromak experiments. Local and global MHD physics issues for magnetic reconnection have been investigated in colliding plasma experiments, utilizing merging of self-sustaining spheromak configurations. Three-dimensional aspects of magnetic reconnection physics have been investigated by axially merging two spheromaks (Yamada et al. 1990, Ono et al. 1993) in the TS-3 (Todai Spheromak-3) devices at the University of Tokyo and at Swarthmore College (Brown 1999, Cothran et al. 2003), and in MRX (Yamada et al. 1997a,b). The 3D features of magnetic reconnection were found to be quite different from the conventional 2D features depending on whether the plasma toroids have cohelicity or counter-helicity configurations.

In the TS-3 experiments (Yamada et al. 1990, Ono et al. 1993), two spheromak-type plasma toroids merge together, contacting and reconnecting along a toroidally symmetric line. In this experiment, the two toroidal spheromaks, which are generated with the same or opposite helicities, carry equal toroidal current with the same or opposite toroidal field. They are called cohelicity merging or counter-helicity merging, respectively. It was found that plasmas of opposite helicity reconnect appreciably faster than those of similar helicity, and the direction of toroidal field plays an important role in the reconnection process. **Figure 11** shows an experimental schematic and the setup for the TS-3 experiment in which two spheromaks of toroidal shape are created and allowed to merge. To document the internal magnetic structure of the reconnection on a single shot, a 2D magnetic probe array is placed on an $R-Z$ plane or toroidal cut-off plane as shown. Evidence of driven reconnection was observed and a quantitative dependence of reconnection rate on external force was documented ($\gamma_{Rec} \propto v$). A 3D plasma acceleration mechanism accompanied by significant ion heating has been indicated during the three-component reconnection process (see Section 4.4.3).

4.4. Recent Major Findings and Discoveries in Lab Plasmas

4.4.1. Signatures of two-fluid physics and reconnection dynamics. The shape of the neutral sheet, or reconnection layer, often manifests the essential physics of the magnetic reconnection process. The Sweet-Parker model assumes resistive MHD description, but gives very slow predictions for the reconnection rates owing to the narrow neutral sheet shown in **Figure 1**. Alternatively, the Petschek model opens up the neutral sheet in a wedge shape as shown in **Figure 2**, leading to a much faster rate of reconnection. But these MHD models have not been verified in collisionless plasmas.

In collisionless reconnection, the MHD framework breaks down in the neutral sheet when its thickness becomes comparable to the ion skin depth for proton $\delta_{i\mathrm{H}}$, as shown in **Figure 4**. Then ions become demagnetized while electrons stay magnetized, leading to various two-fluid effects including the so-called Hall effect owing to separation of ion and electron motions. One of the theoretical predictions of the Hall effect is the presence of a quadrupolar out-of-plane magnetic field (Equation 5). In MRX, these predicted two-fluid signatures have been clearly identified during fast reconnection. **Figure 12*a*,*b*** shows how the profile of the MRX neutral sheet changes with respect to collisionality by comparing the sheet configuration described by the measured magnetic field vectors and flux contours for the high- (collisional) and low-density (nearly collsionless) cases. In the high plasma density case, shown in **Figure 12*a***, where the mean free path is much shorter than the sheet scales, a rectangular shape neutral sheet profile of the Sweet-Parker model is seen, and a classical reconnection rate is measured. In the case of low plasma density, shown in

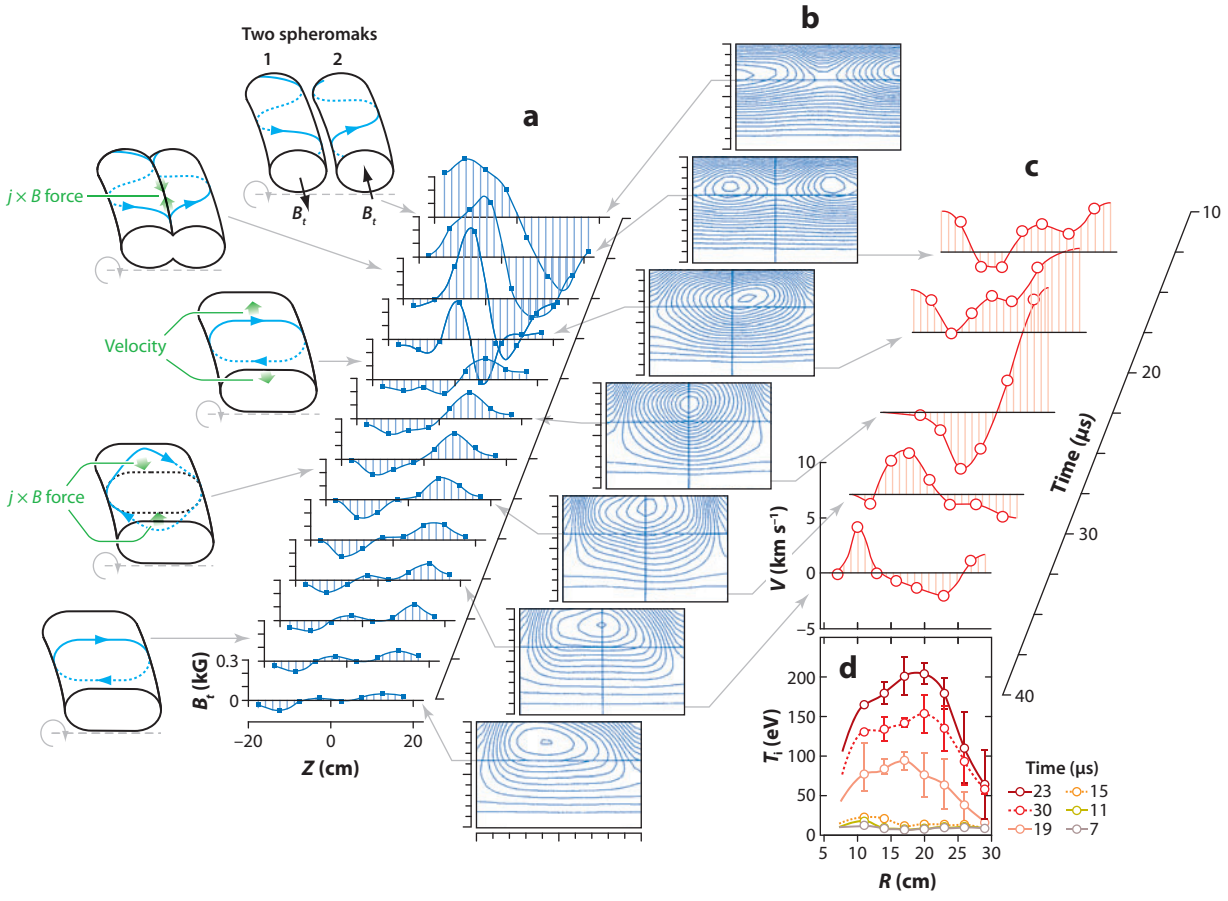

Figure 11

Todai Spheromak-3 experimental schematics and results. (*a*) Axial profiles of the toroidal magnetic field B_t at $r = 18$ cm, (*b*) poloidal flux contours on the $R-Z$ plane, (*c*) radial profiles of the ion global toroidal velocity V_t in the midplane, and (*d*) radial profiles of ion temperature T_i in the midplane during reconnection of two merging spheromaks with equal but oppositely directed B_t. From Ono et al. 1996.

Figure 12*b*, where the electron mean free path is longer than the sheet thickness, Hall effects become dominant, as indicated by the quadrupolar out-of-plane field depicted by the color code. There is no recognizable out-of-plane Hall field in the collisional case as is seen in **Figure 12*a***. Also we note a double-wedge shape sheet profile of Petschek type (shown in **Figure 2**), deviating significantly from that of the Sweet-Parker model (**Figure 1**), and a fast reconnection rate is measured in this low collisionality regime. However, a slow shock, a signature of the Petschek model, has never been identified in this regime to date. This important observation supports the concept that the Hall effects originating from two-fluid dynamics contribute to the significantly enhanced reconnection rate that has been observed in the collisionless reconnection (Ren et al. 2005; Brown, Cothran & Fung 2006; Yamada et al. 2006).

From **Figure 12*b*** (see also **Figure 4**), we can see how two-fluid effects work in the magnetic reconnection region. As the reconnecting fieldlines move into the center of the neutral sheet (the X-point in **Figure 12*b***), ions become demagnetized. As the ion flows change directions gradually by 90°, the electrons still follow the fieldlines until they approach the separatrices or X-point.

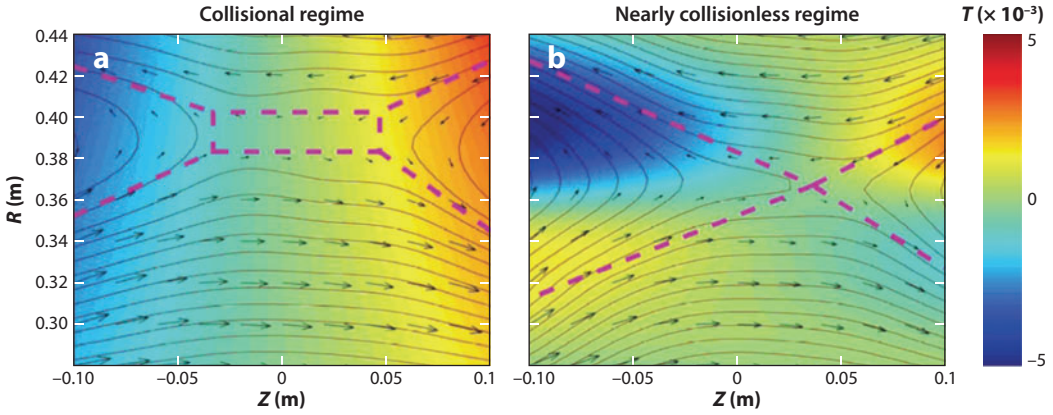

Figure 12

Comparison of magnetic configuration in the reconnection region in two cases: (*a*) collisional regime ($\lambda_{mfp} \sim 1$ mm $\ll$ current sheet thickness), and (*b*) nearly collisionless regime ($\lambda_{mfp} \sim 1$ cm $\sim$ current sheet thickness). In-plane magnetic field is shown by arrows and out-of-plane field is depicted by colors representing -50 ± 50 G. It is clear, as illustrated by dashed pink lines, that the magnetic configuration changes from an elongated current sheet (Sweet-Parker type) to a double-wedge shape (Petschek-like) when reconnection is governed by two-fluid effects. The predicted quadrupole structure of the out-of-plane component is also seen. From Yamada et al. 2006.

Near the X-point the magnetic field weakens and the electron drift [cEy/Bz; an (R, z, y) coordinate system was employed in **Figure 12**)] becomes larger. Finally the electrons are demagnetized and ejected to the exit. This electron flow pattern generates a quadrupolar-shape current profile in the reconnection plane and, thus, creates an out-of-plane magnetic field with a quadrupolar profile. This effect has been regarded as a signature of Hall physics. The increased electric field caused by the strong Hall term ($\boldsymbol{J} \times \boldsymbol{B}$) through a steady, laminar, cross-field current of electrons is translated to a fast motion of flux lines ($E = -d\psi/dt$, where ψ is the flux function) in the reconnection plane, or a fast rate of magnetic reconnection.

4.4.2. Identification of the electron diffusion layer. Utilizing fine-scale magnetic probes, more exact profiles of electron flow have been recently measured. In the neutral sheet of MRX, an electron diffusion region has been identified for the first time in the reconnection layer of a laboratory plasma. The rate of reconnection can be controlled in part by dynamics in this small region, in which magnetic fieldlines tear and reconnect and energy dissipation occurs. The recent 2D numerical simulations of Daughton, Scudder & Karimabadi (2006) and Shay, Drake & Swisdak (2007) predict a two-scale diffusion layer in which an electron diffusion layer resides inside of the larger ion diffusion layer of width the ion skin depth δ_i.

In MRX, the presence of an electron diffusion region was verified and it was found that demagnetized electrons are accelerated in the outflow direction (**Figure 13**). The measured width of the electron diffusion region scales with the electron skin depth ($\sim 8\delta_e$) and the electron outflow scales with the electron Alfvén velocity ($0.11\ v_A$). The general features of both the electron and ion flow structures agree with simulations. But the thickness of the electron diffusion layer is much larger (5 times) than the values obtained by 2D simulations (Pritchett 2001, Daughton, Scudder & Karimabadi 2006). A careful check of collisional effects has been made to determine how much of the enhanced diffusion layer thickness in MRX should be attributed to 3D effects (Ji et al. 2008, Ren et al. 2008) and how much to collisions (W. Daughton & V. Roytershteyn, private communication). Although the electron outflow seems to slow down by dissipation in the electron

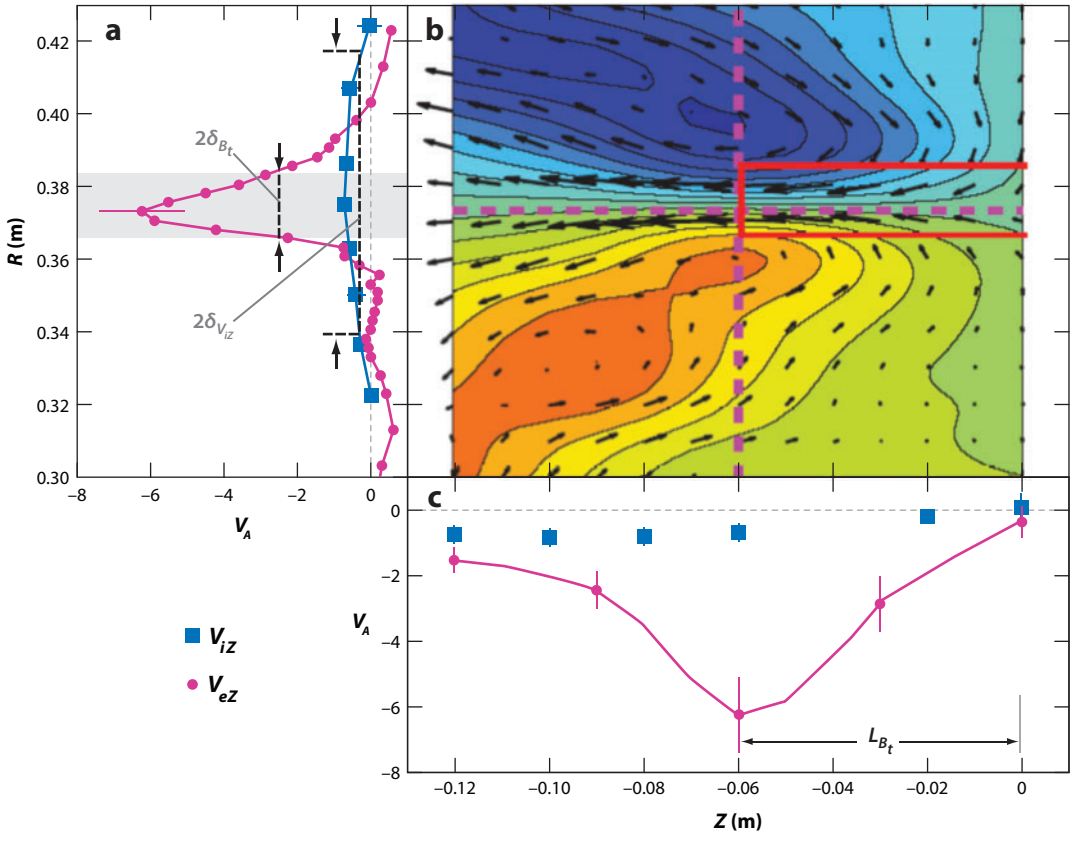

Figure 13

(*a*) The radial profiles of the electron outflow velocity, V_{eZ} (*magenta circles*), and ion outflow velocity, V_{iZ} (*blue squares*), measured in a helium plasma. (*b*) The 2D profile of the out-of-plane field, B_T (*color-coded contours*), and the in-plane electron flow velocity, V_e (*black arrows*); (*c*) V_{eZ} and V_{iZ} as a function of Z. The magenta dashed lines in (*b*) represent the cuts at $Z = -6$ cm and at $R = 37.5$ cm along which the profiles in (*a*) and (*c*) are taken (Ren et al. 2008).

diffusion region, the total electron outflow flux remains independent of the width of the electron diffusion region. We note that even with the presence of the thin electron diffusion region, the reconnection rate is still primarily determined by the Hall electric field, as was concluded by the multicode GEM project (Birn et al. 2001). The ion outflow channel is shown to be much broader than the electron channel, which is also consistent with numerical simulations. Also this electron outflow often occurs impulsively as the collisionality of the plasma is reduced.

4.4.3. Ion heating during plasma merging experiments. One of the most important questions for magnetic reconnection is how magnetic energy is converted into plasma kinetic energy. It was found in recent spheromak merging experiments, in which reconnection is induced by external coil currents (Ono et al. 1996, Brown 1999; see **Figure 11**), that a significant amount of magnetic energy is converted to ion thermal energy during reconnection and that the energy conversion rate is much larger than the value expected from classical dissipation mechanisms.

Strong plasma acceleration and ion heating were documented during counter-helicity merging (**Figure 11*b***). Through time evolution of the poloidal flux contours derived experimentally from

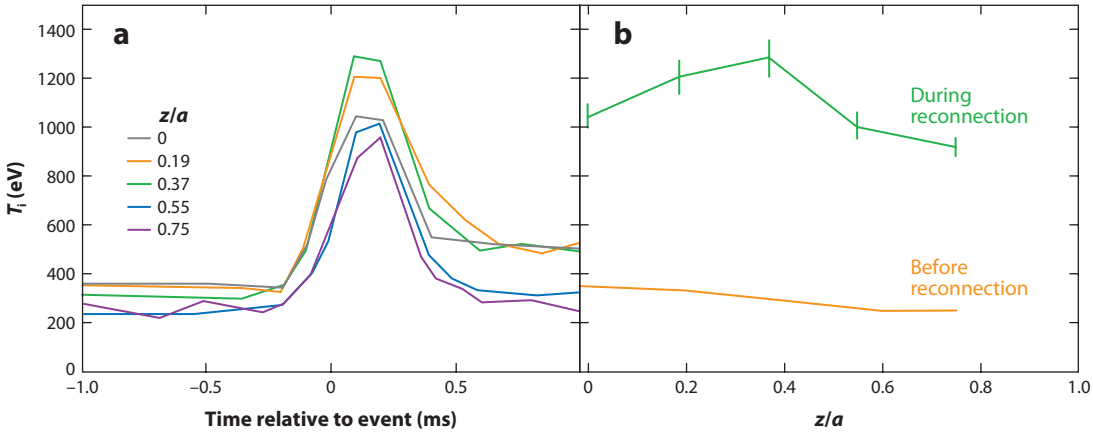

Figure 14

Ion heating in Madison Symmetric Torus. (*a*) Carbon ion temperature versus time at the core. (*a*) Ion temperature versus radius before and during the reconnection event. From Den Hartog et al. 2007.

internal probe arrays, it was found that merging of spheromaks of opposite helicity occurs faster than merging of the same helicity; **Figure 11*a*** depicts the time evolution of profile of toroidal field, B_t, versus Z (axial) direction for counter-helicity merging. Initially, the merging plasmas formed the B_t profile shown in the figure, positive on the left and negative on the right side. As reconnection progressed, the value of B_t decreased as expected but then the B_t profile flipped (changed its polarity) between $t = 20$ and 30 μs. This overshoot is regarded as evidence of the toroidal slingshot effect. Yamada et al. (1990) describe schematically the dynamic 3D evolution of magnetic fieldlines during and after reconnection. Dissipation of Alfvén waves excited by the slingshot motion was identified as the main cause of anomalous ion heating.

4.4.4. Ion heating during reconnection in Reversed Field Pinch. Strong ion heating has been always observed during reconnection in the RFP, but the exact mechanisms have not been determined. Ion heating is particularly strong in the case of multiple reconnection—as shown in **Figure 14**, the temperature quadruples in 100 μs throughout the plasma (Den Hartog et al. 2007) during magnetic self-organization events where magnetic reconnection takes place. The time and radial dependence of the ion temperature through a reconnection event is shown in **Figure 14**. The multiple reconnections occur when an internal reconnection drives multiple tearing modes at the many locations of resonant surfaces. During multiple reconnection there is a notable change in the equilibrium magnetic field topology and a sizable decrease in the stored magnetic energy. It is also observed that impurity ion heating is much stronger than bulk ion temperature rise. Differential heating of minority ions is also observed in the solar wind. The exact reason for this common observation is not identified yet.

4.4.5. Scaling of laboratory data to astrophysics with respect to collisionality. As described earlier in this section, the MRX data suggests that a transition from MHD-like reconnection to collisionless Hall reconnection occurs when the thickness of the reconnection layer becomes comparable to the electron mean free path (Yamada et al. 2006). In the two-fluid regime, the sheet thickness is generally determined by the ion skin depth δ_i. In the one-fluid collisional MHD regime, however, the sheet thickness is determined by the Sweet-Parker width, $L/S^{1/2}$. The ratio

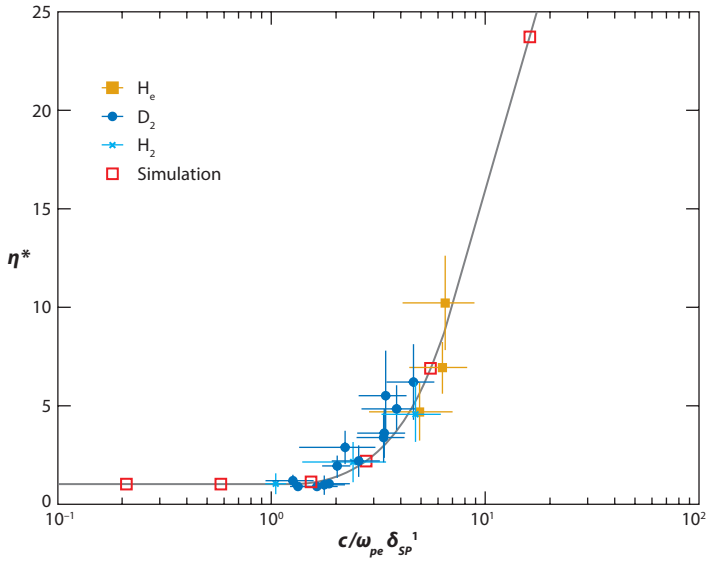

Figure 15

MRX (Magnetic Reconnection Experiment) scaling; effective resistivity $\eta^*(=E/j)$ normalized by the *Spitzer* value η_{SP} versus the ratio of the ion skin depth to the Sweet-Parker width is compared with numerical calculation of the contributions of Hall effects to the reconnection electric field. The simulations were based on a 2D two-fluid code. From Yamada et al. 2006.

of the ion skin depth to the Sweet-Parker layer thickness, δ_{SP}, was shown in Equation 6 to be proportional to $(\lambda_{mfp}/L)^{1/2}$, following Yamada et al. (2006).

In MRX the classical rate of reconnection with the *Spitzer* resistivity is obtained when the resistivity is large enough to satisfy $\delta_i < \delta_{SP}$. When the ion skin depth becomes larger than δ_{SP}, the reconnection layer thickness is expressed by 0.4 δ_i and the reconnection rate is larger than the classical reconnection rate determined by *Spitzer* resistivity. **Figure 15** presents an MRX scaling for effective resistivity $\eta^* = \eta_{eff}/\eta_S$, $(\eta_{eff} \equiv E/j)$ normalized by the *Spitzer* value η_S in the center of the reconnection region. Because in resistive MHD, E is balanced by the Ohmic term in the diffusion region, whereas in two-fluid MHD the Hall term is important as well, η_{eff} represents the effective resistivity generated by two-fluid effects.

The MRX data set is compared with scaling obtained in a recent Hall MHD numerical simulation using a two-fluid MHD code (Breslau & Jardin 2003). The horizontal axis represents the ratio of the ion skin depth to the classical Sweet-Parker width $\delta_{SP} = L/S^{1/2}$, where L was set to be 20 cm, the system scale. **Figure 15** experimentally confirms an important criterion for two-fluid effects to come into play, namely, the reconnection resistivity (or reconnection speed) that takes off from the classical *Spitzer* value (or the Sweet-Parker reconnection rate) when the ion skin depth δ_i becomes larger than twice the Sweet-Parker width δ_{SP}.

The apparent agreement of MRX scaling with a two-fluid Hall MHD (with resistivity included) code has an important implication. It indicates that anomalous resistivity is primarily accounted for by the laminar Hall effect, when the *Spitzer* resistivity is not large enough to balance the large reconnecting electric field in fast magnetic reconnection. Even with the presence of other energy dissipation mechanisms, the reconnection electric field primarily can be represented by the laminar Hall effect, namely, $j_{Hall} \times B$ term, and this is consistent with the MRX data shown in **Figure 15**.

We note that the magnitude of this laminar Hall effect peaks somewhere outside of the X-line. Additional effects, such as anomalous resistivity caused by turbulence, are needed to support reconnection around the X-line and separatrices. It can thus be concluded that both mechanisms, one based on the laminar Hall effect and the other including effects related to turbulence and the electron pressure tensor, are responsible for fast reconnection.

Looking into the future, experimental facilities can be utilized more effectively by widening operation into more astrophysics relevant regimes or by building new devices to address specific physics issues. Study of magnetic reconnection in wide collisionality parameter regime (from $\lambda_{mfp} \ll L$ to $\lambda_{mfp} \gg L$) is desirable. In addition, toroidal fusion experiments, including tokamaks and RFPs, display strong global reconnection phenomena in highly conductive plasmas, and they can be utilized effectively to study magnetic reconnection.

5. THEORY AND SIMULATION OF RECONNECTION

Analytical theory and numerical simulation play complementary roles in the theoretical study of reconnection. Because the range of length scales and timescales in most astrophysical reconnection problems is so large, it is impossible to simulate them directly. Analytical insight has been very important in developing scaling laws and in interpreting simulations as well as data.

This section is organized as follows. The first three subsections treat fast MHD reconnection, two-fluid, or collisionless reconnection, and time-dependent effects, including small-scale instabilities. These topics are in the mainstream of current reconnection research. There are then four subsections on reconnection environments that are especially important in astrophysics (and, to varying degrees, in the laboratory). These are line-tied systems, partially ionized gases, relativistic plasmas, and turbulent plasmas.

5.1. Fast Magnetohydrodynamic Reconnection: Petschek's Theory

We gave a brief discussion of Petschek's theory for fast MHD reconnection in Section 2.2. The theory is based on the fundamental insight that the outflow region can be much broader than the region where the fieldlines actually reconnect. In the fastest Petschek model, the reconnection rate is nearly independent of S and the reconnection rate is nearly v_A.

Petschek reconnection has been shown to be unstable unless η increases near the X-point. The first hint of a problem with the Petschek solution came with attempts to simulate it numerically. Simulations with constant η found that the length of the resistive layer is global, and reconnection proceeds at the slow Sweet-Parker rate (Biskamp 1986). If a Petschek configuration is set up initially, it reverts to Sweet-Parker (Uzdensky & Kulsrud 2000). However, if η is assumed to increase in the resistive layer, Petschek reconnection can be sustained (Ugai & Tsuda 1977; Sato & Hayashi 1979; Scholer 1989; Baty, Priest & Forbes 2006).

Before the importance of a resistivity gradient for the basic geometry of reconnection was appreciated, η was sometimes taken to increase in the resistive layer for computational convenience: This broadens the reconnection region and makes it easily resolved while the outer region remains close to ideal. There is also a physical motivation for enhanced resistivity in the resistive layer: The large current densities there can cause instabilities that effectively enhance the resistivity (so-called anomalous resistivity; Section 5.3.1). Note, however, that because the Coulomb resistivity depends on temperature as $T^{3/2}$, one might expect the intense Ohmic heating in the resistive region to actually reduce η. In any case, owing to these numerical experiments, it is now clear that locally enhanced resistivity has an important effect on the nature of reconnection. Therefore, its use must be justified wherever it is invoked.

In Section 2.2, we argued that if η has a maximum at the X-point a large reconnection angle can be formed (see Equation 3) and reconnection is speeded up. Mathematical models to explain the nonuniform η effect were developed by Kulsrud (2001) and Malyshkin, Linde & Kulsrud (2005), who argued that the resistive layer length L' is determined by the length scale on which η varies.

According to Section 2.4, if the length of the resistive layer L is comparable to the mean free path λ_{mfp}, the MHD treatment of reconnection is invalid. In many astrophysical situations, the maximally fast Petschek model has such a short current sheet that this is indeed the case. Using the results in **Table 1** we see that in a solar coronal loop with global scale L of 10^8 cm and S of 10^{10}, the minimum layer length predicted by Petschek's theory is about 30 cm, whereas λ_{mfp} is $5 \times 10^6\ (T/10^6)^2(10^9/n)$ cm [this appears to be even with anomalous resistivity (Uzdensky 2003)]. In interstellar gas with $L = 10^{18}$ cm, $S = 10^{15}$, $n = 1$, and $T = 10^4$, the minimum Petschek length is about 80 km, while λ_{mfp} is about $R_\odot$. These examples show that even if the local enhancement of η required for Petschek reconnection occurs in astrophysical settings, collisionless effects probably become important before reaching the Petschek scale.

The combination of the breakdown of MHD in the Petschek regime and the requirements on η mean that Petschek reconnection in its original form is unlikely to be the dominant mode of reconnection in astrophysical plasmas. Although his argument that reconnection is fast when the outflow is broader than the resistive layer is one of the most important principles in reconnection theory, much reconnection research today focuses on non-MHD effects.

5.2. Collisionless Reconnection Revisited

In Section 2.4 we gave a brief discussion of collisionless reconnection. The fundamental scale at which the electrons and ions decouple is the ion inertial length, δ_i. (In a high β plasma, the decoupling scale is the ion gyroradius, which exceeds δ_i by a factor of $\beta^{1/2}$.) This can be seen from the equation of motion for a particle of species α,

$$\frac{d\boldsymbol{v}_\alpha}{dt} + \omega_{c\alpha} \times \boldsymbol{v}_\alpha = \frac{q_\alpha}{m_\alpha}\boldsymbol{E}, \tag{8}$$

where $\omega_{c\alpha} \equiv q_\alpha \boldsymbol{B}/m_\alpha c$. Replacing d/dt by a characteristic frequency ω, we see that if $\omega \ll \omega_{c\alpha}$, the second term on the left hand side of Equation 8 dominates. The particle motion is then given by the $E \times B$ drift, $c\boldsymbol{E} \times \boldsymbol{B}/B^2$, independent of particle species; the particles are frozen to the fieldlines, and the MHD approximation applies. If $\omega > \omega_{c\alpha}$, the inertia term dominates and the particles slip off the fieldlines. We use the MHD dispersion relation to estimate the length scale at which this happens for ions: $\omega = \omega_{ci} = kv_A$. According to **Table 1**, this gives $k^{-1} = \delta_i$. As **Table 1** shows, δ_i is generally a microscopic scale in astrophysical plasmas. Equation 6 shows that the thickness of the Sweet-Parker layer drops below δ_i as the length of the current sheet approaches the electron mean free path λ_{mfp}. We argued that this is the criterion for collisionless reconnection. Laboratory measurements indicate that the reconnection rate indeed depends on this criterion, as do simulations by Cassak, Shay & Drake (2005).

We can also express the criterion $\delta_{SP}/\delta_i < 1$ in terms of a critical current sheet length L_c. The 2D profile of the reconnection layer changes drastically as the MRX operation regime is moved from the one regime to the other (Yamada et al. 2006). Using Equation 2 and the definition of S, we find that collisionless effects are important when

$$L < L_c \equiv 4 \times 10^{12} B \left(\frac{T}{n_e}\right)^{3/2}, \tag{9}$$

where all quantities are given in centimeter-gram-second units. In the solar corona, L_c is not too different from typical length scales in coronal loops. This is the basis for the interesting suggestion by Uzdensky (2007) and Cassak, Mullan & Shay (2008) that solar and stellar coronal temperatures and densities are maintained near marginal collisionality through heating by reconnection.

In the interstellar medium, L_c is generally small. Using **Table 1**, if $B = 5\ \mu G$, $T = 10^4$ K, and $n_e = 1\ \mathrm{cm}^{-3}$, then $L_c \sim 2 \times 10^{13}$ cm. Thus, two-fluid effects would only come into play if the reconnecting structure is already very small. In hot, low-density plasmas, such as the gas in galaxy clusters, L_c is much larger. Taking $B = 1\ \mu G$, $T = 10^7$ K, and $n_e = 10^{-3}$ gives $L_c \sim 1\ kpc$. Although this is small on intergalactic scales, it is not too different from the autocorrelation length for turbulence in galaxy clusters measured by Vogt & Ensslin (2003).

The magnetic field and flow configuration in collisionless reconnection are sketched in **Figure 4**. The ions virtually drop out of the flow within about δ_i of the X-point. They do, however, form a neutralizing background that constrains the electron motion, and they contribute to the in-plane current that generates the out-of-plane field (Uzdensky & Kulsrud 2006).

The electron skin depth δ_e is smaller than δ_i by a factor of $\sqrt{m_e/m_i}$, so the electrons remain tied to the fieldlines for a considerable distance after the ions drop out. As magnetic fieldlines approach the X-point, the area per unit flux expands, whereas downstream the area per unit flux contracts. If the electron flow were simply the $E \times B$ drift, n_e would decrease upstream of the X-point and increase downstream. To keep the plasma quasi-neutral, there must be a flow of electrons along the fieldlines. This flow, together with a contribution from the ions at the periphery of the Hall region, constitutes the in-plane current that supports the out-of-plane magnetic field (Uzdensky & Kulsrud 2006).

The area per flux diverges at the X-point and along the separatrices, which divide the plane into regions of distinct magnetic topology. By the continuity argument, $\boldsymbol{J}$ must diverge at these locations. In practice, electron pressure and inertia resolve the singularity, but numerical simulations show that $\boldsymbol{J}$ is indeed large along the separatrices.

The electrons themselves become detached from the fieldlines inside a layer of width δ_e, and their dynamics are dictated by inertia, pressure, and the electric field. It is inside this region that the fluid reconnects.

Numerical simulations show that two-fluid reconnection can be much faster than Sweet-Parker reconnection (Mandt, Denton & Drake 1994; Biskamp, Schwarz & Drake 1995; Ma & Bhattacharjee 1996; Shay & Drake 1998; Birn et al. 2001; Breslau & Jardin 2003). Mandt and colleagues and many subsequent researchers ascribed the difference in rates to Whistler wave versus Alfvén wave physics: Alfvén waves are nondispersive and travel at speed v_A, while the Whistler dispersion relation is $\omega = kv_A(k\delta_i)$. This allows fast propagation on small scales.

For obvious reasons, simulations can only study situations in which the ratio of δ_i to the system size L_g is not too large. The question of how the reconnection rate scales with δ_i/L_g is not yet settled. In particular, it is not clear whether the length L of the outflow region is always L_g or could be a different, shorter length. Numerical simulations and analytical studies of two-fluid reconnection without a guide field and with L assumed to be L_g give a reconnection rate $v_A(\delta_i/L) = v_A(\delta_i/L_g)$ (Mandt, Denton & Drake 1994; Bhattacharjee et al. 2001; Malyshkin 2008). This follows from Sweet-Parker arguments if one simply sets the width of the ion outflow region to δ_i instead of δ_{SP}. However, Shay et al. (1999, 2004) and Huba & Rudakov (2004) argued that the length L of the outflow region always adjusts itself, possibly after a slow development phase (Shay et al. 2004), to about 10 δ_i. Sweet-Parker arguments then give a reconnection rate of 0.1 v_A, independent of L_g. If a guide field is present, it changes the scalings. Wang et al. (2001) found the reconnection rate scales as $(\delta_i/D)^{1/2}$, whereas Fitzpatrick (2004) and Smith et al. (2004) found $(\delta_i/D)^{3/2}$ scaling. It is

important that this question be settled for astrophysical situations, in which δ_i/L_g is typically very small (see **Table 1**).

In summary, reconnection can be faster in collisionless plasmas, but not all astrophysical bodies fall into the collisionless regime. Small, hot systems such as stellar coronae and accretion disks around compact objects are favorable environments for collisionless reconnection. In larger systems such as interstellar and intracluster gas, collisionless reconnection will only occur if the magnetic field is structured on scales far below the macroscopic scales in the system. And, even in situations where collisionless reconnection can be achieved, it is only fast if the inflow speed is relatively independent of the ratio of δ_i to the global scale of the system, L_g.

Finally, we should mention that although early studies attributed the enhanced rate of collisionless reconnection to the Hall effect, it has become less clear that this is the cause. Karimabadi et al. (2004) dropped the Hall term from a simulation in which the ions were treated kinetically and the electrons as a fluid, and still found fast reconnection. Full kinetic simulations of collisionless reconnection in an $e^{\pm}$ plasma, in which there is no Hall effect because all charged particles have the same mass, still find fast reconnection (Bessho & Bhattacharjee 2005, Daughton & Karimabadi 2007).

5.3. Instabilities and Time-Dependent Effects

5.3.1. Anomalous resistivity. The study of secondary instabilities driven by reconnection, and the possibility that feedback from these instabilities could at least sporadically increase the reconnection rate, has a long history and enjoys some observational support, both in natural plasmas and in the laboratory.

Anomalous resistivity, the best known such mechanism for increasing the reconnection rate, describes transfer of electron momentum to small-scale electromagnetic or electrostatic fluctuations, leading to an effective friction force. A simple example of how the ion-acoustic instability leads to anomalous resistivity is worked in Kulsrud (2005). Anomalous resistivity enhances the Sweet-Parker reconnection rate by a factor of $\sqrt{\eta_{anom}/\eta}$, but perhaps more importantly, if η varies with position, Petschek reconnection, the fast alternative to Sweet-Parker reconnection, can occur (Sections 2.2 & 5.1).

Reconnection layers are prime environments because the current density within them is high and gradients in plasma properties such as density are large. Norman & Smith (1978) compiled a set of instabilities that might be an important source of resistivity in reconnecting astrophysical plasmas. To their list should be added lower hybrid drift instabilities, which were originally discussed by Krall & Liewer (1971).

Several types of waves have been detected in reconnecting plasmas. Electromagnetic lower hybrid waves, which have a frequency of order of the lower hybrid frequency $(\omega_{ce}\omega_{ci})^{1/2}$ have been detected in MRX, as have high-frequency electrostatic and electromagnetic waves (Carter et al. 2002, Ji et al. 2004). Lower hybrid waves were observed during reconnection in the Earth's magnetotail (Bale, Mozer & Phan 2002; Cattell et al. 2005), as were whistler waves (Petkaki, Freeman & Walsh 2006; Wei et al. 2007). However, establishing a correlation between the fluctuation level and the reconnection rate, as expected for a simple anomalous resistivity model, has been difficult. The whistlers detected by Ji et al. (2004) do appear to be positively correlated with the reconnection rate in MRX. More detailed studies are needed to find the role of fluctuations in reconnection dynamics. Gekelman, Stenzel & Wild (1982) attributed the enhanced resistivity seen in their reconnection experiment to ion-acoustic waves in plasmas with $T_e/T_i \gg 1$ (if $T_e \sim T_i$, such waves are heavily damped).

Kinetic simulations of microinstabilities in reconnection layers have revealed a complex array of modes that interact nonlinearly with other modes and with the basic state. Some effects of the fluctuations can be described as enhancement of the resistivity (Moritaka, Horiuchi & Ohtani 2007), but the reconnection rate is also affected by electron heating, and by electromagnetic instabilities driven by electrostatic ones, which initially grow faster (Horiuchi & Sato 1999, Lapenta & Brackbill 2002, Daughton, Lapenta & Ricci 2004).

When is anomalous resistivity relevant to astrophysics? Although it is difficult to generalize in such a complex situation, we can say the following. Current-driven instabilities have a threshold electron drift speed $v_D = v_{Dc}$, which is often of order of the ion sound speed (otherwise, the wave energy is absorbed by the thermal ions, preventing net growth). This threshold can be expressed in terms of the width of the current layer as $\delta_c \sim \delta_i(v_A/v_{Dc})$. For $v_{Dc} \sim v_i$ and $v_A/v_i \sim 1$, instability therefore requires $\delta \sim \delta_i$; and the current layer must be thin enough that collisionless effects are important. As we saw in assessing two-fluid effects in astrophysical reconnection, this seems achievable for parameters of stellar coronae, but requires that the interstellar and intergalactic medium be structured on very small scales. Current-driven instabilities, like two-fluid effects, would seem to be most important in small, hot systems.

5.3.2. Evolution of the reconnection layer. Reconnection layers are subject to large-scale instabilities as well as to the microinstabilities discussed in the preceding subsection. These instabilities can modulate the reconnection rate over time, perhaps leading to bursts such as those seen in solar flares.

Instabilities can also create turbulence, which heats and accelerates particles. Detailed discussion of energization methods is beyond the scope of this review, but we mention a few contributions. Acceleration was computed in a model of turbulent MHD reconnection by Ambrosiano et al. (1988) using a test particle approach. More recently, first-order Fermi acceleration of electrons was discussed by de Gouveia dal Pino & Lazarian (2005) and studied in a model of collisionless reconnection by Drake et al. (2006). An enhanced level of electromagnetic fluctuations accompanied by strong ion heating is seen in MST during sawtooth crashes; Tangri, Terry & Fiksel (2008) considered a variety of ion heating mechanisms in this context, but did not find a model that completely explains the data.

The chains of magnetic islands formed by magnetic tearing, depicted in **Figure 3**, can be unstable to coalescing because of the mutual attraction between neighboring current filaments (Finn & Kaw 1977). The outflows in reconnection layers can be unstable to Kelvin-Helmholtz modes, which make them turbulent (Chiueh & Zweibel 1987). Tearing modes can develop in Sweet-Parker reconnection layers (Bulanov, Sakai & Syrovatskii 1979; Biskamp 1993; Malyshkin, Linde & Kulsrud 2005). Daughton, Scudder & Karimabadi (2006) showed in kinetic simulations of collisionless reconnection with open boundary conditions that the electron diffusion region progressively lengthens with time, eventually becoming unstable to forming detached plasmoids that are ejected from the system, leading to an unsteady reconnection rate. Plasmoid formation during MHD reconnection was also discussed by Loureiro, Schekochihin & Cowley (2007).

Despite the importance of these fluctuations in determining how a reconnecting system evolves, they do not remove the bottleneck imposed by long MHD reconnection timescales. This problem must be addressed by other processes, and is a topic of intense current debate.

5.4. Reconnection in Line-Tied Systems

Magnetic fieldlines in the coronae of stars and accretion disks are rooted in the dense, highly conducting gas below. In the limit of infinite conductivity and infinite density contrast, the corona

can be treated as an isolated system with a rigid lower boundary at which the fieldlines are tied. Certain laboratory experiments (Bellan, You & Hsu 2005; Bergerson et al. 2006) replicate line-tied boundary conditions as well.

The constraint of zero-perturbed velocity on the boundary turns out to have a strong effect on reconnection. In Section 2.3 we remarked that spontaneous magnetic tearing occurs at locations where the local MHD–restoring forces vanish, permitting otherwise weak resistive effects to dominate. For a single Fourier harmonic of the form $e^{i\boldsymbol{k}\cdot\boldsymbol{x}}$, the tearing condition is satisfied on surfaces $\boldsymbol{x}_s$ where $\boldsymbol{k}\cdot\boldsymbol{B}(\boldsymbol{x}_s) \equiv 0$. [For example, in a cylinder with a twisted field $\boldsymbol{B} = \hat{\theta}B_\theta(r)+\hat{z}B_z(r)$, a single Fourier harmonic would have the spatial form $e^{ik_z z+im\theta}f(r)$ and tearing layer would be at r_s defined by $k_z B_z(r_s)+mB_\theta(r_s)/r_s = 0$.] But a single Fourier harmonic cannot satisfy zero boundary conditions.

The effect of line-tying on tearing modes in cylinders with helical magnetic fields and slabs with sheared fields have recently been studied by Delzanno & Finn (2008) and Huang & Zweibel (2009), respectively. In both cases, it is found that instability is completely suppressed if the length of the systems is less than a critical value L_c, which is independent of resistivity and is typically about 100 times the scale a on which $\boldsymbol{B}$ varies horizontally. As L is increased above L_c, perturbations that grow at the resistive rate (growth time proportional to the Lundquist number S) are found, but it is unclear whether such slowly growing modes should be called instabilities at all. Finally, at a value of L that depends on S as $S^{2/5}$ there is a transition to tearing mode scaling, with the growth time proportional to $S^{3/5}$. Tearing mode scaling is restored when the system is so long that it is possible to construct superpositions of Fourier modes with nearly the same r_s. In practice, the loops are then so long—$L/a > 10^3$—that coronal tearing modes should be effectively suppressed. This argues that another mechanism initiates reconnection in line-tied magnetic fields.

5.5. Reconnection in Weakly Ionized Gases

Much of the interstellar gas in disk galaxies is only weakly ionized. The ionization fraction in the so-called warm neutral medium is about 0.01, in molecular clouds it is about 10^{-7}, and in protostellar disks it can be as low as 10^{-10}. The photospheres of late-type stars are also weakly ionized.

Partial ionization affects reconnection in several ways. The effect on electrical conductivity is perhaps the most obvious. Coulomb collisions dominate electron-neutral collisions up to densities of $\sim 10^{7-8}$ cm^{-3} (Zweibel 1999), and S is generally high in the interstellar medium. Protoplanetary disks are a notable exception, in that the combination of low conductivity and small size allows S to fall below unity (Hayashi 1981). The magnetic field is then so weakly coupled to the gas that reconnection becomes a meaningless concept. An intermediate regime, in which neutral collisions are important in modifying the conductivity but the magnetic field is still coupled to the medium, was considered by Wardle & Ng (1999).

The level of ionization also enters the reconnection rate through the Alfvén speed. For perturbations on timescales much longer than the ion-neutral collision time τ_{in}, the operational definition of v_A is $B/\sqrt{4\pi(\rho_i+\rho_n)}$, that is, the plasma and neutrals move together. For perturbations on timescales much shorter than the ion-neutral collision time $\tau_{in} = (\rho_i/\rho_n)\tau_{ni}$, the plasma and the neutrals are decoupled and the characteristic Alfvén speed is $B/\sqrt{4\pi\rho_i}$. The effect of partial ionization on MHD tearing mode growth rates was calculated by Zweibel (1989). On small length scales, where the plasma and neutrals are decoupled, the tearing mode growth rate is increased by a factor of $(\rho_n/\rho_i)^{1/5}$ owing to the dependence on Alfvén speed.

A related but larger enhancement of the reconnection rate can occur in plasmas with short recombination times. Recall that Sweet-Parker reconnection is slow because all the gas brought

into the thin resistive layer must be expelled at a speed not exceeding v_A. Defining an outflow time $t_{flow} \equiv L/v_A$, Equation 2 for the inflow velocity can be written as $v_{in} = (\lambda/t_{flow})^{1/2}$. If only the plasma flows into the resistive layer, leaving the neutrals behind, and the resulting excess ions recombine on a timescale $t_{rec} \ll t_{flow}$, the reconnection rate can be approximated by $v_{in} \sim (\lambda/t_{rec})^{1/2}$ (Heitsch & Zweibel 2003a, Lazarian et al. 2004; the former paper gives a slightly different result that accounts for ion pressure). This type of reconnection is related to the tendency to form thin current layers in weakly ionized gas (Brandenburg & Zweibel 1994). However, a guide field, even a weak one, suppresses fast reconnection, because the magnetic field convected toward the reconnection layer must also be expelled, and, unlike the plasma, is not eliminated by recombination (Heitsch & Zweibel 2003b).

Finally, adding neutrals to a plasma pushes the Hall effect to a larger scale. The effective inertia of the ions increases owing to collisions with the neutrals, with the result that the ion skin depth δ_i increases to $\delta_i \sqrt{\rho_n/\rho_i}$. Although simulations of reconnection that include both the Hall effect and collisions with neutrals have not yet been carried out, it is at least possible that fast reconnection will set in at this larger scale.

5.6. Reconnection in Relativistic Plasmas

Magnetic energy extracted by reconnection in relativistic plasma has been considered an energy source in pulsar winds (Coroniti 1990, Lyubarsky & Kirk 2001), giant flares in the magnetospheres of magnetars (Thompson & Duncan 1995, 2001; Lyutikov 2006), gamma-ray bursts (Drenkhahn & Spruit 2002), and jets from active galactic nuclei (Romanova & Lovelace 1992). Most studies of relativistic reconnection assume that the so-called magnetization parameter σ_m, the ratio of magnetic to plasma energy density (including rest mass energy), is very large. Blackman & Field (1994) considered relativistic versions of Sweet-Parker and Petschek reconnection models and pointed out that the Lorentz contraction of the outflow with respect to the inflow would increase its density, thus allowing a greater inflow rate. A more complete solution to the relativistic Sweet-Parker problem was found by Lyutikov & Uzdensky (2003), who showed that if σ_m exceeds the Lundquist number S, the inflow speed can be relativistic. This was corroborated by Watanabe & Yokoyama (2006), who carried out relativistic MHD simulations of reconnection with a locally enhanced resistivity.

Tearing mode instability in the relativistic regime was considered by Komissarov, Barkov & Lyutikov (2007). They were able to map the problem onto standard MHD and showed that the resistivity dependence of the tearing mode growth rate is similar to that in nonrelativistic plasmas.

In Section 5.2, we alluded to kinetic simulations of reconnection in pair plasmas. Reconnection in relativistic pair plasmas has recently been considered by a number of researchers, beginning with Zenitani & Hoshino 2001 (see also Jaroschek, Lesch & Treumann 2004; Zenitani & Hesse 2008). A common feature of these works is that the reconnection rate is relativistic, and the reconnection electric field is so strong that particles in the diffusion region can be accelerated to high energies or heated to high temperatures (Zenitani & Hoshino 2007). This makes reconnection an attractive candidate for a fast energy release mechanism, and a fast particle acceleration mechanism, in these systems.

5.7. Reconnection in Turbulent Plasmas

Many astrophysical plasmas are turbulent, so the question of how turbulence affects reconnection has long been of interest. If turbulence with a small scale l and velocity v is present in a large-scale reconnection layer, one might imagine that the magnetic diffusivity η is replaced by a much larger

effective diffusivity of order lv. Matthaeus & Lamkin (1985, 1986) treated this problem in a series of 2D numerical experiments on a magnetic null layer with initial random perturbations. They found time-dependent, bursty reconnection, but no evidence that the overall average reconnection rate of the layer was affected by turbulence. Strauss (1988) showed that tearing mode turbulence can act as a hyper-resistivity, which increases the rate of reconnection on a scale much larger than the turbulent scale. Later, Kim & Diamond (2001) carried out analytical calculations of turbulent reconnection in so-called reduced MHD, in which a strong guide field makes the dynamics nearly 2D. They argued that the back reaction of the magnetic field on the turbulence would suppress turbulent diffusion, leaving the reconnection rate proportional to $\lambda^{-1/2}$, as it is for slow MHD reconnection. Both groups of researchers noted that 2D MHD and reduced 3D MHD have strong conservation laws that constrain turbulence and its interaction with reconnection, but that the reconnection rate in a full 3D treatment might be quite different.

Lazarian & Vishniac (1999) reconsidered reconnection in which a spectrum of small-scale, 3D turbulence extending to the resistive scale is present. They argued on analytical grounds that the reconnection rate should be independent of λ and could reach v_A. The main effects that enhance the reconnection rate are the presence of many magnetic X-points and the rapid divergence of neighboring magnetic fieldlines, which permits the mass flux away from the null points to be larger than it is for the nearly straight fieldlines characteristic of Sweet-Parker geometry. Numerical experiments on reconnection of a large-scale sheared magnetic field with forced turbulence suggest that reconnection is faster than in a laminar system, and the reconnection rate increases with increasing turbulent amplitude (Kowal, Lazarian & Vishniac 2009). This problem remains an exciting area for investigation.

6. GLOBAL EFFECTS IN RECONNECTION

In the next three subsections we address three interrelated issues. The first is how the small-scale structure that seems so necessary for fast astrophysical reconnection can be produced. The second is how reconnection can be driven. The third is the effect of reconnection on the global configuration and is related to the phenomenon of self-organization.

6.1. Formation of Small-Scale Structure

Fast reconnection requires structure on scales shorter than a mean free path, or small enough to trigger microinstabilities that provide anomalous resistivity, or otherwise limit the length of the diffusion region. The problem of how to introduce these scales into systems with much larger global scales is one of the fundamental issues in this subject. In addition, in some applications, such as flares in stellar and accretion disk coronae and sawtooth crashes in laboratory plasmas, reconnection must remain coupled to global energy reservoirs. Three types of mechanism have been considered. Although detailed examination of any of them would take us beyond the scope of this review, a brief discussion is warranted because of the importance of this problem.

In laboratory plasmas, the explanation focused on instabilities that lead to reconnection at the nonlinear stage. One such example is the internal kink mode of a plasma column with a helical magnetic field. Rosenbluth, Rutherford & Dagazian (1973) and Waelbroeck (1989) showed that in the nonlinear state, this mode has a helical current sheet that can rapidly reconnect, possibly initiating a sawtooth disruption (see **Figure 6**). Longcope & Strauss (1993) showed that an array of adjacent parallel and antiparallel magnetic flux tubes can be unstable to coalescence, and that the nonlinear outcome of the instability is an equilibrium with current sheets. Some researchers have reported numerical evidence that such current sheets develop in line-tied plasmas as well

(Gerrard & Hood 2004, Browning et al. 2008), but it is not clear that their relatively simple topology avoids the constraints on current sheet formation derived by van Ballegooijen (1988) and Cowley, Longcope & Sudan (1997).

In systems that are highly dynamical and not strongly influenced by boundaries, such as the interstellar medium and accretion disks, attention has focused on turbulent cascades. Turbulence produces thin current sheets or filaments, which can reconnect. Examples are given by Frank et al. (1996); Malagoli, Bodo & Rosner (1996); and Palotti et al. (2008) for the case of an initially uniform, weak magnetic field wound up by shear flow turbulence. There would be no reconnection if the field were not stirred up by turbulence. Shear flow can also enhance the rate of reconnection in situations that would be unstable to tearing (Knoll & Chaćon 2002).

In stellar and accretion disk coronae, in which the fieldlines are tied at a boundary, filamentation of the current driven by boundary motions is a likely mechanism for producing small-scale structure. The original scenario for this process is due to Parker (1972), who argued that when the footpoints of the coronal magnetic fieldlines are displaced by random motions in the dense lower atmosphere, the field is generally unable to reach a smooth equilibrium. Instead, discontinuities develop where the current density is infinite. (Of course, resistivity, no matter how small, precludes infinite current, but what matters is that the current would be infinite in an ideal medium and very large in a medium with high S.) Later, Parker's suggestion was generalized to include the possibility that the current does not actually become singular, but rather grows indefinitely (van Ballegooijen 1988, Longcope & Strauss 1994). Other work (Syrovatskii 1981, Low & Wolfson 1988, Zweibel & Proctor 1990, Longcope & Cowley 1996, Titov & Démoulin 1996, Low 2006) considered current sheet formation in more complex magnetic topologies. These latter studies are based on the result that a magnetic null point can become a current sheet if perturbed and that discontinuous changes in the footpoint connectivity of the magnetic fieldlines are natural locations for current singularities caused by shear.

Numerical simulations of the Parker problem (Galsgaard & Nordlund 1996) show that as random motions tangle the magnetic field, the current becomes increasingly filamented. Relaxation events, in which the current is dissipated and the magnetic field is rearranged on dynamical, not resistive, timescales occur continuously at a low level, but can also be large and violent. It is desirable to identify this process with heating and flaring in the corona. A major open question is how the rate, statistics, and other properties of the energy release scale with Lundquist number S. Simulations show that if S is increased, the contribution of the highest current density points to the total power output is also increased. Because the range of S accessible in computations is four orders of magnitude or more below solar values of S, and because collisionless effects so far not included in the computations may play a role, it is difficult to apply this work quantitatively to the Sun. Whatever the precise details of the process, it appears that a progressive complexification of line-tied magnetic fields by random footpoint motions creates current concentration on small scales, and this may be the key to rapid reconnection where it is otherwise difficult to understand.

6.2. Driven Reconnection

Reconnection is said to be driven when it occurs only because of external forcing. A typical example is a series of colliding plasma experiments that have been carried out for more than a decade (Yamada et al. 1990, Ono et al. 1993, Brown 1999). In studying the merger of two self-sustaining spheromak configurations, it is found that the reconnection rate exceeds the Sweet-Parker rate and depends on the external driving force through the colliding velocity (Yamada et al. 1990). In MRX, reconnection is driven in a controlled manner by pulsing programmed currents in the external

coils (Yamada 1997a,b). The axisymmetric ($m = 0$) tearing mode in MST is another example: It is stable, but can be excited in the presence of unstable $m = 1$ modes (Choi et al. 2006). The reconnection of colliding magnetic flux tubes studied analytically by Zweibel & Rhoads (1995) and numerically by Linton, Dahlburg & Antiochos (2001) is another example. Because many astrophysical systems are highly dynamical, the driven reconnection problem is highly relevant to astrophysics.

An important question is how driven reconnection is related to spontaneous reconnection. Although a general answer to this question is lacking, there is one well-studied case in which it is not: the so-called Taylor problem originally studied by Hahm & Kulsrud (1985). In the Taylor problem, a sheared magnetic field, $\boldsymbol{B} = \hat{y}B_y(x) + \hat{z}B_z(x)$; $B_y(0) = 0$, $|B_y/B_z| \ll 1$, is in equilibrium between two plates at $x = \pm a$. The magnetic profile is stable to tearing. Then, at time $t = 0$, the boundaries are given a small, antisymmetric ripple $\xi(x = a, y) = -\xi(x = -a, y) = \epsilon a \cos ky$, where $\epsilon \ll 1$, and $ka \ll 1$, which pushes opposing fields together along the midplane. To first order in ϵ, there are two possible equilibria for the rippled slab. In one, the current is finite everywhere, but there is a chain of islands. In the other, the magnetic topology has changed, but there is a current sheet at the midplane. Hahm & Kulsrud showed that the system tends initially to the singular equilibrium, but then enters a resistive phase in which the fieldlines reconnect and the system approaches the equilibrium with magnetic islands. For large Lundquist numbers $S \geq 10^4$, the peak reconnection rate scales as $S^{-3/5}$. Thus, we find that the rate of driven reconnection approaches the spontaeous reconnection rate of tearing modes (Vekstein 2004).

6.3. Reconnection and Self-Organization

Self-organization refers to the spontaneous transition of a system from one equilibrium state to another, usually initiated by an instability. Because the frozen flux condition is a very strong constraint on the equilibria available to a system, magnetic self-organization usually involves reconnection. As discussed in Section 4, sawtooth relaxation events in tokamak and RFP plasmas are typical examples. Sawtooth relaxation in tokamaks involves a relatively small amount of magnetic flux change, but causes a large drop in the central electron temperature, which is attributed to magnetic reconnection. Reversed field pinch formation is perhaps one of the best studied examples of magnetic self-organization in the laboratory. RFPs are formed with a toroidal field of constant sign: The development of a field reversal is entirely due to internal processes. A heuristic explanation for the reversed state was provided by Taylor (1974), who postulated that systems in force-free equilibrium seek the lowest energy state compatible with fixed magnetic helicity K (see Equation 7). Self-organization according to this principle is called Taylor relaxation. Studies of relaxation in MST show that self-organization comes about through the joint action of a few global tearing modes (Sykes & Wesson 1977), and that magnetic energy is dissipated while helicity is approximately conserved, in agreement with Taylor's theory (Ji et al. 1995).

Taylor relaxation has also been invoked as a heating mechanism in the solar corona (Browning & Priest 1986, Browning et al. 2008), where it is assumed that random motions in the photosphere drive the field away from a Taylor state, and energy is released when it relaxes back. The reconnection rate is taken as a free parameter in these theories: If it is too fast, energy cannot build up; but if it is too slow, little energy is released.

Up to now, theories of self-organization have applied mainly to systems that are magnetically dominated. This is the case for most laboratory plasmas. In astrophysics, it is chiefly true in stellar and accretion disk coronae. Self-organization in high β or moderate β systems has achieved less attention and is not as well understood.

7. SUMMARY AND INVENTORY OF UNSOLVED PROBLEMS

Magnetic reconnection is a fundamental process in plasma physics. Because the large Lundquist number S of most astrophysical systems otherwise precludes resistive behavior such as dissipation of magnetic flux, it is also a key process in astrophysics. It extracts magnetic energy from the system to power laboratory sawtooth crashes and astrophysical flares, and it provides the changes in magnetic topology necessary for magnetic self-organization processes, including dynamos and Taylor relaxation. Laboratory experiments, detailed observations of solar flares, in situ measurements in space plasmas, numerical simulation, and theory all provide a good platform for studying reconnection.

We briefly described several reconnection models. The Sweet-Parker theory, an MHD theory characterized by long, thin current sheets, slow inflows, and Alfvénic outflows, is slow because all the fluid brought into the resistive layer must be expelled at v_A through a narrow channel. This continuity problem appeared to be resolved in Petschek's MHD theory by making the current sheet shorter and diverting the fluid by shocks. But Petschek reconnection seems to be realizable only if the plasma resistivity η increases toward the annihilation region. Although Petschek-like flow can, however, be attained in collisionless reconnection, the fundamental physics is quite different, and the ion dynamics do not allow a shock structure. Other ways around the continuity problem arising in Sweet-Parker theory include relativistic boosts (Section 5.6), plasma recombination (Section 5.5), and turbulent spreading of the fieldlines (Section 5.7).

The long-standing question of why reconnection occurs so fast in collisionless plasmas has been addressed in light of two-fluid physics. Hall MHD effects were verified in numerical simulations as well as in both laboratory and space plasmas. In the collisional regime, the Sweet-Parker model has been verified by numerical simulations and by laboratory experiments. The reconnection rate is found to increase rapidly as the ratio of the electron mean free path to the scale length increases. This result is attributed to the large Hall electric field in the reconnection layer except near the X-point where a strong dissipation mechanism takes place.

A continuing theme in this review is that in order for any of the fast reconnection theories to operate in astrophysics, there must be mechanisms for producing small-scale structure—whether to decouple electrons and ions, as is necessary in collisionless reconnection (Section 5.2), sustain the high current densities necessary for anomalous resistivity (Section 5.3.1), or avoid the unfavorable scaling of the reconnection rate with the global length scale predicted by some theories. Although we gave only a short synopsis of such mechanisms (Section 6.1), the need for them should not be forgotten.

There are several problems that require further study. We need a more complete understanding of the structure and dynamics of the electron dissipation region, where magnetic fieldlines are broken. The consensus of the GEM challenge project (Birn et al. 2001) was that the reconnection rate is governed by the Hall term in the generalized Ohm's law. However, this term does not provide energy dissipation. In recent studies using particle in cell (PIC) codes, we have learned that energy dissipation in the neutral sheet would occur in a small region, leading to a much smaller rate of energy conversion from magnetic to particle kinetic energy. This rate is too small to explain the observed particle heating during reconnection observed in RFP plasma relaxation events, in spheromak merging experiments, or in solar flare evolution.

At the moment, there is no clear conclusive theory of how magnetic energy is converted to plasma kinetic energy. We do not yet know the role of fluctuations, how they are excited, and how they determine the reconnection rate by influencing energy conversion processes. It is very important to investigate the relationship between anomalous particle acceleration and reconnection rates. This is also essential for predicting the observational signatures of reconnection, including

ion velocity profiles and spectroscopic signatures of the electron distribution function. These are cornerstones of diagnosing reconnection in astrophysical environments.

We need a better understanding of how reconnection couples to the global system. Although many difficulties involving solar flare energetics would be alleviated by multiple reconnection sites triggered nearly simultaneously and impulsively, we do not yet know how this occurs. Is there any general criterion or reason why magnetic energy is stored for a long period and then suddenly released, driving the plasma to a globally relaxed state? Is the relationship between the local reconnection rate and the buildup of global stored energy a key? Can fast collisionless reconnection operate in systems with macroscopic size much larger than the mean free path, as is often the case in astrophysics?

The magnetic self-organization of plasma is influenced and determined both by local plasma dynamics in the reconnection region and by global boundary conditions in 3D global topology. It has been found in laboratory plasmas that a large MHD instability caused by external conditions can often produce a current layer that undergoes magnetic reconnection and can determine its rate. In this area, major progress can be made by experimentally investigating the key features of magnetic self-organization of laboratory plasmas and by comparing the results from the rapidly advancing advanced numerical simulations.

We need a more detailed understanding of reconnection in the particular circumstances that often apply to astrophysical but not laboratory plasmas—relativistic plasmas, weakly ionized gases, and systems that are not magnetically dominated, but contain strong flows, both ordered and turbulent.

Collaboration between theorists and experimentalists can answer these questions. Improved understanding of the physics of magnetic reconnection should provide astrophysicists with tools to develop theories of flares, astrophysical dynamos, γ-ray bursts, and evolution of accretion disks, and to interpret their observational signatures. Given the current rate of progress, we are optimistic about further development on all of these problems.

DISCLOSURE STATEMENT

The authors are not aware of any affiliations, memberships, funding, or financial holdings that might be perceived as affecting the objectivity of this review.

ACKNOWLEDGMENTS

We are happy to acknowledge many of our colleagues in the Center for Magnetic Self-Organization, as well as Jim Drake, Terry Forbes, Hugh Hudson, Max Lyutikov, and Jennifer Stone for advice and help. This work was supported in part by NSF Grants AST0507367, PHY0215581, and PHY0821899 to the University of Wisconsin and PHY0551164 to the University of California, Santa Barbara. We are grateful to the KITP, where part of this review was written, for hospitality.

The authors apologize for not covering many fine works because of the limitation of space for this brief review of magnetic reconnection.

LITERATURE CITED

Adler EA, Kulsrud RM, White RB. 1980. *Phys. Fluids* 23:1375
Aly JJ. 1984. *Ap. J.* 283:349
Ambrosiano J, Matthaeus WH, Goldstein ML, Plante D. 1988. *J. Geophys. Res.* 93:14383
Aschwanden MJ. 2002. *Space Sci. Rev.* 101:1

Aschwanden MJ. 2008. *Ap. J.* 672:L135
Balbus A, Hawley JF. 1998. *Rev. Mod. Phys.* 70:1
Bale SD, Mozer FS, Phan T. 2002. *Geophys. Res. Lett.* 29:33–1
Bastian TS, Benz AO, Gary DE. 1998. *Annu. Rev. Astron. Astrophys.* 36:131
Baty H, Priest ER, Forbes TG. 2006. *Phys. Plasmas* 13:022312
Baum PJ, Bratenahl A. 1974. *Phys. Fluids* 17:1232
Bellan PM. 2000. *Spheromaks*. London: Imperial College Press
Bellan PM, You S, Hsu SC. 2005. *Astrophys. Space Sci.* 298:203
Bergerson W, Forest C, Fiksel G, Hannum D, Kendrick R, et al. 2006. *Phys. Rev. Lett.* 96:015004
Bessho N, Bhattacharjee A. 2005. *Phys. Rev. Lett.* 95:245001
Bhattacharjee A. 2004. *Annu. Rev. Astron. Astrophys.* 42:365
Bhattacharjee A, Ma ZW, Wang X. 2001. *Phys. Plasmas* 8:1829
Birn J, Drake JF, Shay MA, Rogers BN, Denton RE, et al. 2001. *J. Geophys. Res.* 106:3715
Biskamp D. 1986. *Phys. Fluids* 29:1520
Biskamp D. 1993. *Nonlinear Magnetohydrodynamics*. Cambridge, UK: Cambridge Univ. Press
Biskamp D, Schwarz E, Drake JF. 1995. *Phys. Rev. Lett.* 75:3850
Blackman EG, Field GB. 1994. *Phys. Rev. Lett.* 72:494
Brandenburg A, Zweibel EG. 1994. *Ap. J.* 427:L91
Braginskii SI. 1965. *Rev. Plasma Phys.* 1:205
Bratenahl A, Yeates CM. 1970. *Phys. Fluids* 13:2696
Breslau J, Jardin SC. 2003. *Phys. Plasmas* 10:1291
Brown MR. 1999. *Phys. Plasmas* 6:1717
Brown MR, Cothran CD, Fung J. 2006. *Phys. Plasmas* 13:056503
Browning PK, Gerrard C, Hood AW, Kevis R, Van Der Linden RAM. 2008. *Astron. Astrophys.* 485:837
Browning PK, Priest ER. 1986. *Astron. Astrophys.* 159:129
Bruhwiler DL, Zweibel EG. 1992. *J. Geophys. Res.* 97:10825
Bulanov SV, Sakai J, Syrovatskii SI. 1979. *Sov. J. Plasma Phys.* 5:157
Bulanov SV, Sasorov PV. 1975. *Astron. Zh.* 52:763
Carter TH, Ji H, Trintchouk F, Yamada M, Kulsrud RM. 2002. *Phys. Rev. Lett.* 88:015001
Cassak PA, Mullan DJ, Shay MA. 2008. *Ap. J.* 676:L69
Cassak PA, Shay MA, Drake JF. 2005. *Phys. Rev. Lett.* 95:235002
Cattell C, Dombeck J, Wyant J, Drake JF, Swisdak M, et al. 2005. *J. Geophys. Res.* 110:A01211
Charbonneau P, McIntosh SW, Liu H-L, Bogdan TJ. 2001. *Solar Phys.* 203:321
Chiueh T, Zweibel EG. 1987. *Ap. J.* 317:900
Choi S, Craig D, Ebrahimi F, Prager SC. 2006. *Phys. Rev. Lett.* 96:145004
Ciaravella A, Raymond JC. 2008. *Ap. J.* 686:1372
Coroniti FV. 1990. *Ap. J.* 349:538
Cothran CD, Landreman M, Brown MR, Matthaeus WH. 2003. *Geophys. Res. Lett.* 30:1213
Cowley SC, Loncope DW, Sudan R. 1997. *Phys. Rep.* 283:227
de Gouveia dal Pino EM, Lazarian A. 2005. *Astron. Astrophys.* 441:845
Daughton W, Karimabadi H. 2007. *Phys. Plasmas* 14:072303
Daughton W, Lapenta G, Ricci G. 2004. *Phys. Rev. Lett.* 93:105004
Daughton W, Scudder J, Karimabadi H. 2006. *Phys. Plasmas* 13:072101
Delzanno GL, Finn JM. 2008. *Phys. Plasmas* 15:032904
Den Hartog DJ, Ahn J-W, Almagri AF, Anderson JK, Beklemishev AD, et al. 2007. *Nucl. Fusion* 47:17
Dennis BR. 1985. *Solar Phys.* 100:465
Dennis BR, Hudson HS, Krucker S. 2007. *Lect. Notes Phys.* 725:33
Drake JF, Swisdak M, Che H, Shay MA. 2006. *Nature* 443:553
Drenkhahn G, Spruit HC. 2002. *Astron. Astrophys.* 391:1141
Egedal J, Fasoli A, Nazemi J. 2003. *Phys. Rev. Lett.* 90:135003
Egedal J, Fasoli A, Porkolab M, Tarkowski D. 2000. *Rev. Sci. Instrum.* 71:3351
Emslie AG, Kucherek H, Dennis BR, Gopalswamy N, Holman GD, et al. 2004. *J. Geophys. Res.* 109:A10104
Eriksson S, Elkington SR, Phan TD, Petrinec SM, Reme H, et al. 2004. *J. Geophys. Res.* 109:A12203

Finn JM, Kaw PK. 1977. *Phys. Fluids* 20:72
Fitzpatrick R. 2004. *Phys. Plasmas* 11:937
Fletcher L, Hudson HS. 2008. *Ap. J.* 675:1645
Forbes TW, Priest ER. 1982. *Planet Space Sci.* 30:1183
Frank A, Jones TW, Ryu D, Gaalaas JB. 1996. *Ap. J.* 460:777
Frank AG. 1974. *Izdatel'stvo Nauka, Moscow*, pp. 108–66
Friedman M. 1969. *Phys. Rev.* 182:1408
Fromang S, Papaloizou J, Lesur G, Heinemann T. 2007. *Astron. Astrophys.* 476:1123
Furth HP, Killeen J, Rosenbluth MN. 1963. *Phys. Fluids* 6:459
Galeev AA, Rosner R, Vaiana GS. 1979. *Ap. J.* 229:318
Galsgaard K, Nordlund A. 1996. *J. Geophys. Res.* 101:13445
Gekelman W, Stenzel R, Wild N. 1982. *J. Geophys. Res.* 87:101
Gerrard CL, Hood AW. 2004. *Solar Phys.* 223:143
Goodman J, Uzdensky D. 2008. *Ap. J.* 688:555
Gosling JT, Phan TD, Lin RP, Szabo A. 2007. *Geophys. Res. Lett.* 34:L15110
Gosling JT, Skoug RM, McComas DJ, Smith CW. 2005. *Geophys. Res. Lett.* 32:L05105
Güdel M. 2004. *Astron. Astrophys. Rev.* 12:71
Hahm TS, Kulsrud RM. 1985. *Phys. Fluids* 28:2412
Haisch B, Strong KT, Rodono M. 1991. *Annu. Rev. Astron. Astrophys.* 29:275
Hayashi C. 1981. *Prog. Theor. Phys. Suppl.* 70:35
Heitsch F, Zweibel EG. 2003a. *Ap. J.* 583:229
Heitsch F, Zweibel EG. 2003b. *Ap. J.* 590:291
Horiuchi R, Sato T. 1999. *Phys. Plasmas* 6:4565
Huang Y-M, Zweibel EG. 2009. *Phys. Plasmas* 16:042102
Huba J, Rudakov L. 2004. *Phys. Rev. Lett.* 93:175003
Hudson HS. 2009. *Heliophysics II. Energy Conversion Processes*, ed. CJ Schrijver, GL Siscoe. In press
Hurley K, Boggs SE, Smith DM, Duncan RC, Lin R, et al. 2005. *Nature* 434:1098
Inoue Y, Totani T, Ueda Y. 2008. *Ap. J.* 672:L5
Jaroschek CH, Lesch H, Treumann RA. 2004. *Ap. J.* 605:L9
Ji H, Almagri A, Prager S, Sar J. 1994. *Phys. Rev. Lett.* 73:668
Ji H, Prager SC, Sarff JS. 1995. *Phys. Rev. Lett.* 74:2945
Ji H, Ren Y, Yamada M, Dorfman S, Daughton W, Gerhardt SP. 2008. *Geophys. Res. Lett.* 35:L13106
Ji H, Terry S, Yamada M, Kulsrud R, Kuritsyn A, Ren Y. 2004. *Phys. Rev. Lett.* 92:115001
Ji H, Yamada M, Hsu S, Kulsrud RM. 1998. *Phys. Rev. Lett.* 80:3256
Ji H, Yamada M, Hsu S, Kulsrud RM, Carter T, Zaharia S. 1999. *Phys. Plasmas* 6:1743
Jing J, Qiu J, Lin J, Qu M, Xu Y, Wang H. 2005. *Ap. J.* 620:1085
Kadomtsev B. 1975. *Sov. J. Plasma Phys.* 1:389
Karimabadi H, Krauss-Varban D, Huba JD, Vu HX. 2004. *J. Geophys. Res.* 109:A09205
Kaspi VM, Gavril FP, Woods PM, Jensen JB, Roberts MSE, Chakrabarty D. 2003. *Ap. J.* 588:L93
Kim E-J, Diamond PH. 2001. *Ap. J.* 556:1052
Klimchuk JA. 2006. *Solar Phys.* 234:41
Knoll DA, Chacón L. 2002. *Phys. Rev. Lett.* 88:215003
Knox SO, Barnes CW, Marklin GJ, Jarboe TR, Henins I, et al. 1986. *Phys. Rev. Lett.* 56:842
Komissarov SS, Barkov M, Lyutikov M. 2007. *MNRAS* 374:415
Kowal G, Lazarian A, Vishniac ET. 2009. *Ap. J.* In press
Krall NA, Liewer PC. 1971. *Phys. Rev. A.* 4:2094
Kulsrud RM. 2001. *Earth Planets Space* 53:417
Kulsrud RM. 2005. *Plasma Physics for Astrophysics*. Princeton, NJ: Princeton Univ. Press
Lapenta G, Brackbill J. 2002. *Phys. Plasmas* 9:1544
Lazarian A, Vishniac ET. 1999. *Ap. J.* 517:700
Lazarian A, Vishniac ET, Cho J. 2004. *Ap. J.* 595:812
Lee J, Gary DE, Choe GS. 2006. *Ap. J.* 647:638
Levinton FM, Batha SH, Yamada M, Zarnstorff MC. 1993. *Phys. Plasmas B* 5:2554

Lin J, Ko Y-K, Sui L, Raymond JC, Stenborg GA, et al. 2005. *Ap. J.* 622:1251
Linton MG, Dahlburg RB, Antiochos SK. 2001. *Ap. J.* 553:905
Lites BW. 2000. *Rev. Geophys.* 38:1
Longcope D, Cowley SC. 1996. *Phys. Plasmas* 3:2885
Longcope D, Strauss HR. 1993. *Phys. Fluids B* 5:2858
Longcope D, Strauss HR. 1994. *Ap. J.* 437:851
Loureiro NF, Schekochihin A, Cowley SC. 2007. *Phys. Plasmas* 14:100703
Low BC. 1996. *Solar Phys.* 167:217
Low BC. 2006. *Ap. J.* 649:1064
Low BC, Wolfson R. 1988. *Ap. J.* 324:574
Lu ET, Hamilton RJ. 1991. *Ap. J.* 380:L89
Lyubarsky Y, Kirk JG. 2001. *Ap. J.* 547:437
Lyutikov M. 2003. *MNRAS* 346:540
Lyutikov M. 2006. *MNRAS* 367:1594
Lyutikov M, Uzdensky D. 2003. *Ap. J.* 589:893
Ma ZW, Bhattacharjee A. 1996. *Geophys. Res. Lett.* 23:1673
Malagoli A, Bodo G, Rosner R. 1996. *Ap. J.* 456:708
Malyshkin L. 2008. *Phys. Rev. Lett.* 101:225001
Malyshkin L, Linde T, Kulsrud RM. 2005. *Phys. Plasmas* 12:102902
Mandt ME, Denton RE, Drake JF. 1994. *Geophys. Res. Lett.* 21:73
Masuda S, Kosugi T, Hara H, Tsuneta S, Ogawara Y. 1994. *Nature* 371:495
Matthaeus WH, Lamkin SL. 1985. *Phys. Fluids* 28:303
Matthaeus WH, Lamkin SL. 1986. *Phys. Fluids* 29:2513
Miller KA, Stone JM. 2000. *Ap. J.* 534:398
Moritaka T, Horiuchi R, Ohtani H. 2007. *Phys. Plasmas* 14:102109
Mozer FS, Bale SD, Phan TD. 2002. *Phys. Rev. Lett.* 89:015002
Murphy RJ. 2007. *Space Sci. Rev.* 130:127
Nagayama Y, McGuire KM, Bitter M, Cavallo A, Fredrickson ED, et al. 1991. *Phys. Rev. Lett.* 67:3527
Nagayama Y, Yamada M, Park W, Fredrickson ED, Janos AC, et al. 1996. *Phys. Plasmas* 3:1647
Nita GM, Gary DE, Lanzerotti LJ, Thomson DJ. 2002. *Ap. J.* 570:423
Norman CA, Smith RA. 1978. *Astron. Astrophys.* 68:145
Ono Y, Ellis RA Jr, Janos AC, Levinton FM, Mayo RM, et al. 1988. *Phys. Rev. Lett.* 61:2847
Ono Y, Morita A, Katsurai M, Yamada M. 1993. *Phys. Plasmas* 4:1953
Ono Y, Yamada M, Akao T, Tajima T, Matsumoto R. 1996. *Phys. Rev. Lett.* 76:3328
Palotti ML, Heitsch F, Zweibel EG, Huang Y-M. 2008. *Ap. J.* 678:234
Parker EN. 1957. *J. Geophys. Res.* 62:509
Parker EN. 1972. *Ap. J.* 174:499
Parker EN. 1990. *Geophys. Res. Lett.* 17:2055
Paschmann G, Sonnerup BUO, Papamastorakis I, Schopke N, Haerendel G, et al. 1979. *Nature* 282:243
Petkaki P, Freeman MP, Walsh AP. 2006. *Geophys. Res. Lett.* 33:L16105
Petschek HE. 1964. *NASA Spec. Publ.* 50:425
Phan TD, Gosling JT, Davis MS, Skoug RM, Øieroset M, et al. 2006. *Nature* 439:175
Phan TD, Paschmann G, Twitty C, Mozer FS, Gosling JT, et al. 2007. *Geophys. Res. Lett.* 34:L14104
Pneuman GW. 1981. In *Solar Flare Magnetohydrodynamics*, ed. ER Priest, p. 379. London: Gordon & Breach
Priest ER, Forbes TW. 2000. *Magnetic Reconnection: MHD Theory and Application*. Cambridge, UK: Cambridge Univ. Press
Priest ER, Forbes TW. 2002. *Astron. Astrophys. Rev.* 10:313
Pritchett PL. 2001. *J. Geophys. Res.* 106:3783
Ramaty R, Mandzhavidze N. 2000. *Highly Energetic Physical Processes and Mechanisms for Emission from Astrophysical Plasmas, IAU Symp. 195*, ed. PCH Martens, S Tsuruta, MA Weber, p. 123. San Francisco: Astron. Soc. Pac.
Ren Y, Yamada M, Gerhardt SP, Ji H, Kulstrud R, Kuritsyn A. 2005. *Phys. Rev. Lett.* 95:055003
Ren Y, Yamada M, Ji H, Gerhardt SP, Kulstrud RM. 2008. *Phys. Rev. Lett.* 101:085003

Retinò A, Sundkvist D, Vaivads A, Mozer F, André M, Owen CJ. 2007. *Nat. Phys.* 3:235
Reynolds RJ, Haffner LM, Tufte SL. 1999. *Ap. J.* 525:L21
Romanova M, Lovelace RVE. 1992. *Astron. Astrophys.* 262:26
Rosenbluth MN, Rutherford PH, Dagazian RY. 1973. *Phys. Fluids* 16:1894
Rosner R, Golub L, Vaiana GS. 1985. *Annu. Rev. Astron. Astrophys.* 23:413
Rutherford PH. 1973. *Phys. Fluids* 16:1903
Sarff J, Almagri A, Anderson J, Brower D, Craig D, et al. 2005. In *The Magnetized Plasma in Galaxy Evolution*, ed. KT Chyzy, K Otmianowska-Mazur, M Soida, R-J Dettmar, pp. 48–55
Sato T, Hayashi T. 1979. *Phys. Fluids* 22:1189
Scholer M. 1989. *J. Geophys. Res.* 94:8805
Schrijver CJ, DeRosa ML, Metcalf T, Barnes G, Lites B, et al. 2008. *Ap. J.* 675:1637
Schwartz SJ, Zane S, Wilson RJ, Pijpers FP, Moore DR, et al. 2005. *Ap. J.* 627:L129
Shay MA, Drake JF. 1998. *Geophys. Res. Lett.* 25:3759
Shay MA, Drake JF, Rogers BN, Denton RE. 1999. *Geophys. Res. Lett.* 26:2163
Shay MA, Drake JF, Swisdak M. 2007. *Phys. Rev. Lett.* 99:155002
Shay MA, Drake JF, Swisdak MM. 2004. *Phys. Plasmas* 11:2199
Smith D, Ghosh S, Dmitruk P, Matthaeus WH. 2004. *Geophys. Res. Lett.* 31:L02805
Soltwisch H. 1988. *Rev. Sci. Instrum.* 59:1599
Stenzel R, Gekelman W. 1979. *Geophys. Phys. Res.* 86:649
Strauss HR. 1988. *Ap. J.* 326:412
Sturrock PA. 1991. *Ap. J.* 380:655
Su Y, Gan WQ, Li YP. 2006. *Solar Phys.* 238:61
Sweet PA. 1958. In *Electromagnetic Phenomena in Cosmic Physics*, ed. B Lehnert, p. 123. London: Cambridge Univ. Press
Sykes A, Wesson JA. 1977. In *Proc. 8th Eur. Conf. Control. Fusion Plasma Phys*. Prague. 1:80 Czech Acad. Sci.
Syrovatskii SI. 1981. *Annu. Rev. Astron. Astrophys.* 19:163
Taylor JB. 1986. *Rev. Mod. Phys.* 28:243
Taylor JB. 1974. *Phys. Rev. Lett.* 33:1139
Tangri V, Terry PW, Fiksel G. 2008. *Phys. Plasmas* 15:112501
Thompson C, Duncan RC. 1995. *MNRAS* 275:255
Thompson C, Duncan RC. 2001. *Ap. J.* 561:980
Titov VS, Démoulin P. 1999. *Astron. Astrophys.* 351:707
Tsuneta S. 1996. *Ap. J.* 456:840
Ugai M, Tsuda T. 1977. *J. Plasma Phys.* 17:337
Uzdensky D. 2003. *Ap. J.* 587:450
Uzdensky D. 2007. *Phys. Rev. Lett.* 99:262101
Uzdensky D, Goodman J. 2008. *Ap. J.* 682:608
Uzdensky D, Konigl A, Litwin C. 2002. *Ap. J.* 565:1205
Uzdensky D, Kulsrud RM. 2000. *Phys. Plasmas* 7:4018
Uzdensky D, Kulsrud RM. 2006. *Phys. Plasmas* 13:062305
van Ballegooijen A. 1988. *Geophys. Astrophys. Fluid Dyn.* 41:181
Vekstein G. 2004. *Phys. Plasmas* 11:3525
Veronig A, Temmer M, Hanslmeier A, Otruba W, Messerotti M. 2002. *Astron. Astrophys.* 382:1070
Vogt C, Ensslin TA. 2003. *Astron. Astrophys.* 412:373
Waelbroeck FL. 1989. *Phys. Fluids B* 1:2372
Wang X, Bhattacharjee A, Ma Z. 2001. *Phys. Rev. Lett.* 87:265003
Wardle M, Ng C. 1999. *MNRAS* 303:239
Watanabe N, Yokoyama T. 2006. *Ap. J.* 647:L123
Wei XH, Cao JB, Zhou GC, Santolik O, Rème H, et al. 2007. *J. Geophys. Res.* 112:A10225
Wesson J. 1987. *Tokamaks*. London: Clarendon Press
Woltjer L. 1958. *Proc. Natl. Acad. Sci. USA* 44:489
Yamada M. 2007. *Phys. Plasmas* 14:058102
Yamada M, Furth HP, Hsu W, Janos A, Jardin S, et al. 1981. *Phys. Rev. Lett.* 46:188

Yamada M, Ji H, Hsu S, Carter T, Kulsrud R, et al. 1997a. *Phys. Plasmas* 4:1936
Yamada M, Ji H, Hsu S, Carter T, Kulsrud R, et al. 1997b. *Phys. Rev. Lett.* 78:3117
Yamada M, Kulsrud RM, Ji H. 2008. *Rev. Mod. Phys.* In press
Yamada M, Levinton F, Pomphrey N, Budny R, Manickam J, Nagayama Y. 1994. *Phys. Plasmas* 1:3269
Yamada M, Ono Y, Hayakawa A, Katsurai M, Perkins FW. 1990. *Phys. Rev. Lett.* 65:721
Yamada M, Ren Y, Ji H, Breslau J, Gerhardt S, et al. 2006. *Phys. Plasmas* 13:2119
Zenitani S, Hesse M. 2008. *Ap. J.* 684:1477
Zenitani S, Hoshino M. 2001. *Ap. J.* 562:L63
Zenitani S, Hoshino M. 2007. *Ap. J.* 670:702
Zweibel EG. 1989. *Ap. J.* 340:550
Zweibel EG. 1999. *Phys. Plasmas* 6:1725
Zweibel EG, Haber DA. 1983. *Ap. J.* 264:648
Zweibel EG, Proctor MRE. 1990. In *Topological Fluid Mechanics*, ed. HK Moffatt, p. 187. Cambridge, UK: Cambridge Univ. Press
Zweibel EG, Rhoads J. 1995. *Ap. J.* 440:407

Annual Review of Astronomy and Astrophysics

Volume 47, 2009

Contents

Indexes

Errata

An online log of corrections to *Annual Review of Astronomy and Astrophysics* articles may be found at http://astro.annualreviews.org/errata.shtml